EMG ACTIVITY DETECTION AND CONDUCTION VELOCITY ESTIMATION FROM CAPACITIVE MEASUREMENTS.

Relatore:
Prof. Lorenzo Chiari

Presentata da:
Gabriele Borelli

Correlatore:
Dr. Jochen Damerau

Abstract

The development of robust and reliable tools able to detect muscles' electromyographic (EMG) activity and to assess user's force intention would bring about strong improvements in human-machine interfaces. Current EMG-based solutions are unpractical and they can not be operated by unexperienced users. In the first place, an off-line algorithm able to reliably detect EMG activity through contact-less measurements was developed and tested with experimental data. Performance comparable to algorithm based on direct-contact-EMG-acquisitions were obtained. Further, a capacitive-sensing array-based EMG acquisition system composed of sensors, hardware and software was designed and realized. Performance were tested through two different experimental setups. In the first case the system performed in line with the theory and with state-of-the-art EMG acquisition systems. In the second case, uncontrolled influencing factors affected the measurements, and results were not statistically significant. Performance are strongly encouraging and further tests need to be done to proof the effectiveness and robustness of the designed system. It was concluded that EMG activity detection and user's force intention are possible to assess through contact-less EMG acquisitions without any skin preparation, nor manual calibration, nor accurate electrodes positioning, and over a layer of clothing.

Contents

List of Figures

List of Tables

Introduction

The purpose of the present work is investigating new tools for wearable-device-control systems based on electromyographic (EMG) signals. These tools, software or hardware, must be reliable and suitable to non-clinical environment, e.g. normal-life conditions. In particular, applications without the need of exact electrodes positioning and without a direct contact with the skin, but over clothes, are investigated. The developing of an easy-to-use and robust system able to detect EMG's features without any preparation nor manual calibration, but wearable as a garment, would bring about important improvements in human-machine interfaces.

The dissertation started from analyzing EMG signals acquired through a working acquisition system. This device is a capacitive-sensing EMG acquisition system developed by Ueno et al. [12]. It is able to acquire EMG signals through a thin layer of clothing with an acceptable signal-to-noise ratio (SNR). Two tools have been developed from the starting condition. The first target of the research is an EMG-activity-detection algorithm. The algorithm should be able to detect EMG activations from contactless EMG datasets recorded through the system described in [12]. Moreover, the algorithm should have performance comparable to the algorithms developed for classic surface EMG acquisition systems. The second target of the study is a new EMG acquisition system composed of hardware and software. The aim of this second system should be the estimation of muscle fibers' conduction velocity (CV), and consequently the qualitative investigation of a relationship between the CV and the force generated by the studied muscle. This new ac-

quisition system should include an hardware part able to detect EMG signals through the capacitive-sensing technique; a software part is also necessary. The algorithm should be able to estimate the average CV of the investigated muscle. Finally, the system should enable the studying of a relationship between CV and the entity of muscle contraction. The dissertation is organized in four chapters. The first one aims to provide the reader with some simple background theory related to EMG signals. The information reported in chapter one will be useful in the reading of the thesis. The second chapter regards the first target that was addressed in the research: the EMG-activity-detection algorithm. It includes the description of methods, results and their discussion. This chapter has been submitted to the open access journal *Sensors* for its publication. The title of the study is: *Automatic detection of EMG activity from capacitive measurements*, and the authors are: Jovana Jovic[1] , Yoel Rosales[1] , Gabriele Borelli[1] , Koichi Matsuda[1] , Akinori Ueno[2] and Jochen Damerau[1]. The third chapter addresses the second target of the thesis: the developing of a new capacitive-sensing EMG acquisition sytem for muscle fibers' conduction velocity estimation. The chapter includes the description of methods, results and their discussion. A particular focus has been given to the developed electrodes because a patent application about them has been written and submitted. The title of the patent is: *Capacitive electrode array for electromyography* and the inventors are: Gabriele Borelli[1] and Jochen Damerau[1]. Chapter four collects the conclusions about the dissertation and resumes the results. At the end of the dissertation two appendixes are available. Appendix A describes with more details the design of the electronic board developed in chapter three. Appendix B focuses on the force visual feedback system used in the experimental setup of chapter three.

---

[1]Bosch Corporation Japan, Tokyo, Japan.

[2]Department of Electronics and Computer Engineering, Tokyo Denki University, Ishizaka, Hatoyama-machi, Saitama, Japan.

Chapter 1

Background

Any human activity, from a slight gesture to physical exercise, requires muscle contractions to achieve the desired movement, or to maintain a desired posture. These muscle contractions are the final result of a complex series of tasks: motion planning, generation of muscle control signals, and monitoring of sensory information to allow appropriate corrections of the original plan. Once the decision to move a body segment is made an electrical signal called action potential will be generated and transmitted along spinal nerves and muscle fibers causing muscle contractions [1]. The electromyographic (EMG) signal is a biomedical signal that is composed of action potentials. EMG signals are often used by clinicians as a diagnostic tool [2] especially in fields of orthopedic surgery [3] and rehabilitation [4, 5, 6]. In addition EMG signals can be used in the area of assistive and rehabilitation robotics for the control of assistive devices such as active exoskeletons and prostheses [7, 8, 9].

1.1 The origin of EMG signals

In the study and acquisition of EMG signals, their genesis process and some of their composing elements must be known. The main unit of the EMG signal is the action potential. This unit is an electrical potential transmitted from the nervous system to the controlled muscle. Initially, the signal

travels through the motor neuron (MN) and reaches the muscles in the point of innervation between the MN and the muscle. Then, the signal propagates through the muscle fibers that are innervated by the considered MN. The group composed of motor neuron and innervated muscle fibers is called motor unit (MU). The propagation happens along the fibers in two opposite direction starting from the point of innervation, and it brings about the contraction of the innervated fibers. Action potentials are sent to muscle fibers at specific frequency in order to properly control muscle's contraction. Action potentials travel at different speed during their path. In the first place, the conduction velocity (CV) of motor neuron lies in the order of 50-100 m/s. Then, the CV falls under 10 m/s when the action potential propagates through muscle fibers. Moreover, different kind of fibers are characterized by different conduction velocities. When a specific level of force is requested to the muscle, two main mechanism are used by the nervous system to reach the desired level of contraction: modulation of firing rates and recruitment of new motor units. As reported in [10], these two control methods act simultaneously to obtain smooth movements and a smooth force control. Two simplified rules are:

- The higher the requested force, the higher the firing rate.

- The higher the requested force, the higher the number of recruited motor units.

The recruitment method is largely more complex than the two mentioned points, but they enable the reader to understand the meaning of conduction velocity and its application in the force estimation. According to Henneman et al. [11], new motor units are recruited with a specific order: larger MUs have a higher recruitment threshold than smaller ones. Thus, small motor units are recruited in the first place and, only with the increasing of the requested force, large motor units are gradually involved. The former are characterized by a smaller CV than the latter. Hence, the possibility of measuring muscle's average CV (defined as the the mean CV over the recruited

MUs) could bring about the estimation of a feature related to muscle's force. The described MU recruiting strategy is also known as Henneman's principle.

1.2   EMG signal acquisition

Muscle activity can be recorded by two main types of electrodes: needle electrodes and surface electrodes. Needle electrodes enable the detection of the EMG signal of single motor units. They consist of disposable needles that are injected directly into the muscle of the subject and they contact the MU under investigation. This procedure brings about several limits. To begin with, an experienced staff is necessary to setup an EMG acquisition. Further, the subject can perform a limited set of movements because of the discomfort created by the injected needles. Finally, it is not possible to devise long-term acquisition because of the high invasiveness. Surface EMG (sEMG) recording is a common method of EMG acquisition because it is non-invasive and it can be conducted by personnel other than medical doctors with minimal risk for subjects. However when used for long period of time, also the sEMG technique can cause irritation and discomfort to subjects, and it is a potential cause of skin allergy and inflammation [12]. In addition, surface electromyography requires time consuming skin preparation each time the system is used. Usually, it is necessary to shave subject's skin and to use a specific conductive gel in order to be able to acquire a reliable signal. Recently, Ueno et al. have developed capacitive EMG electrodes capable of sensing muscle activation signals through a thin layer of clothing [12]. The technique has been successfully used to acquire electrocardiographic [12] and electromyographic [14] signals. Morevoer, capacitive EMG acquisition does not require any kind of skin preparation nor any conductive gel. The drawback of contactless EMG sensing is the low signal-to-noise ratio. The body-electrode capacitance acts as a coupling capacitor with magnitude of tens of pico-Farads. Such coupling capacitance significantly varies with motion, pressure or other mechanical factors [15]. However, the proper algorithm could account for

capacitive sensing drawbacks, as shown in the present work.

1.3 State-of-the-art commercial acquisition systems

To the best of author's knowledge, no commercial applications of EMG capacitive-sensing acquisition systems can be found on the market. Only few works in literature regards contactless EMG sensors, such as [12] [16, 17]. Conversely, different kinds of contact sEMG acquisition systems are available and in some cases mentioned in the literature. For instance [62] exploits some products from "Ottino Bioelettronica" (Torino) and from "LISiN-Prima Biomedical & Sport" (Treviso). EMG signal applications are often bound to the availability of a suitable acquisition system. In fact, only a limited amount of information can be acquired through single differential acquisition systems. The estimation of further feature, such as CV, requires more advanced tools. Linear electrode array is a piece of technology that enable a deeper investigation of EMG signals. As reported in [18], several applications, that were unfeasible with single electrode pair, become possible with linear electrode array. The natural evolution of linear electrode array is bidimensional electrode array. A matrix of electrodes can perform even more sophisticated analyses, as explained in [18]. Different applications could rely on sEMG technology, such as mentioned at the beginning of the present chapter, but they need a high reliability and low usage complexity in order to enter the consumer market. Human interface machine is a strong research field, and its market is expected to grow from US$3.9 billions (2015 value) to US$11 billions (2024 estimated value), as reported from "Transparency Market Research".

Chapter 2

EMG Activity Detection

For years, the detection of EMG activation has been conducted using a visual inspection of EMG signals or comparison of EMG amplitude to a fixed threshold value, i.e. when the signal overcomes the pre-set threshold, a muscular activation is reported. Those approaches are becoming less and less used because they are time consuming and not feasible for real-time control of assistive devices [20]. Therefore, in the past decades research effort focused on improving threshold based EMG detection. Methods based on EMG processing techniques, such as full wave amplitude rectification and low pass filtering [21, 22], and algorithms based on statistical properties of EMG signals, such as the double-threshold algorithm [22, 23, 24] and the generalized likelihood ratio test [25], have been proposed. The detailed review of mentioned algorithms can be found in [20]. Despite the improvements in detection techniques, the above mentioned algorithms are based on EMG amplitude analysis, which is subject specific and might change over time due to electrode misallocation, muscle fatigue appearance and other factors. In addition, they require manual adjustment of the threshold value for each user. To cope with this problem, algorithms based on time-frequency analysis of EMG signals have been proposed. In 2003, Merlo and coworkers [26] proposed a method for the identification of single motor unit action potentials based on the wavelet transformation (WT). Since then, many applications of

7

WT in EMG processing have been proposed. Examples of such applications are analysis of combat sports and martial arts strikes [27], characterization of lower back pain [28], detection of muscle fatigue [29], determination of muscle contraction during human walking [30] and identification of hand motion [31, 32, 33, 34, 35, 36]. For the analyses of EMG signals, De Luca used fast Fourier transform (FFT) [37]. FFT can be used only in case of stationary signals, hence its application to EMG analyses is limited due to the variations in muscle force, length and contraction speed, [38, 39]. Compared to FFT, short time Fourier transform (STFT) is a less restrictive method, since it requires that the signal is stationary only within its moving window. Studies have shown that STFT and WT give comparable results regarding detection of muscle fatigue in both static and dynamic exercises [38, 40]. In this study, the STFT is proposed for detection of muscle activation recorded using contactless EMG sensors. The novelty of the approach is in the application of short time Fourier transform and the spectral distance (SD) method to overcome difficulties in processing EMG signal recorded using contactless EMG electrodes. In particular, our attention was focused on extracting a feature independent from the amplitude of the signal, which we could rely on to detect EMG activation. Spectral distance is a numerical measure of the dissimilarity of two spectral shapes, thanks to the introduced normalization, it is not related to the amplitude of the signal or the amplitude of the noise. In addition, to the best of author's knowledge, spectral distance measure has not been used before for detection of EMG activation.

2.1   Methods

The proposed system for detection of EMG activation is shown in Figure 2.1. The acquisition system is schematically shown in the upper part of the figure. Surface EMG signals are acquired through two contactless electrodes. Then, the electrical signals pass into an impedance transformer which serves as a buffer. Finally, a differential amplifier stage is used in order to differenti-
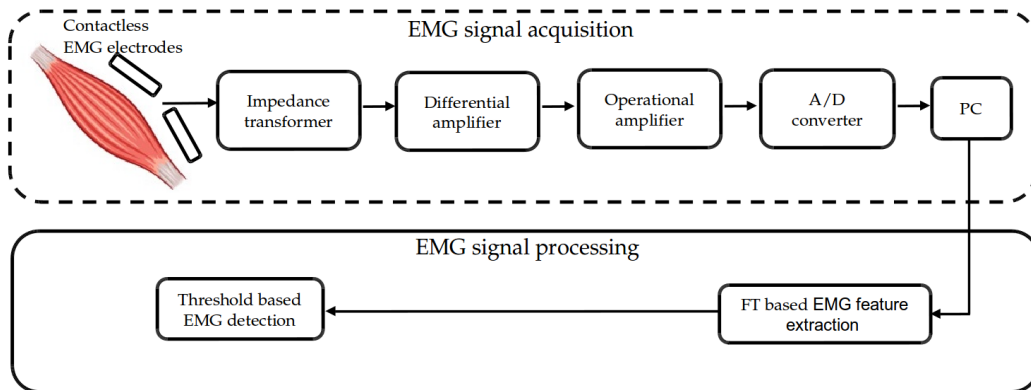
Figure 2.1: Schematic representation of the proposed system for EMG detection. Muscle representation is adapted from [41].

ate signals from each of the contactless electrodes. Signals are then amplified, converted to digital signals and stored into a personal computer (PC) for offline processing. The software EMG processing algorithm, represented in Figure 2.1 in the lower frame, is composed of the Fourier-Transform-based EMG feature extraction block, and the threshold-based EMG detection block. The latter reports muscular activation when the input of EMG detection function is higher than the pre-set threshold value. Each block of the proposed system for detection of EMG activation is discussed in more details below.

2.1.1   Capacitive Electrodes and Acquisition System

The signal is acquired through an electrode made of conductive and flexible fabric. Using a flexible material is very important in order to achieve a closer fit of the electrodes to the measured surface. Figure 2.2, adapted from [42], depicts the model of two capacitive electrodes coupled to the skin.

As it is shown in Figure 2.1, the output signal from the electrodes is the input of the impedance transformer. The impedance transforming circuit is a voltage follower that provides impedance matching between the output impedance of electrodes, which is considerably high due to its capacitive nature, and the input impedance of the rest of the circuit. Figure 2.3 shows
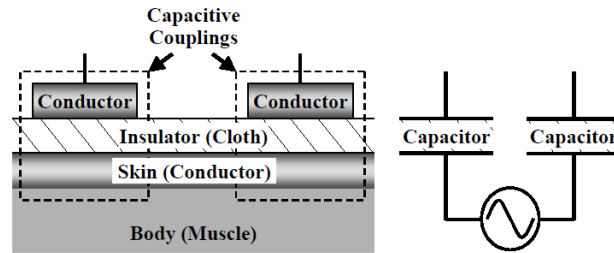
Figure 2.2: Schematic model of two capacitive electrodes coupled to the skin. Adapted from [13].

the remaining components in the signal acquisition system. The circuit comprises an instrumentation amplifier INA 121, an inverter amplifier OP07, and an extra OP07 for AC-coupling of the differential circuit. The AC-coupling helps to reduce the effect of the motion artifacts and of the low frequency components. Consequently, the acquired signal is filtered with a 5th order Butterworth high-pass filter with a cut-off frequency of 20 Hz and implemented via software. The cut-off frequency was chosen in accordance with what has been proved in [57].

The introduction of additional hardware filters, such as comb filters, has been avoided in order to reduce the total signal delay. In fact, reducing the time latency between the EMG activity and the detection is critical in most of EMG activity detection applications.

2.1.2   EMG processing algorithm

The algorithm is divided in two parts: *Fourier-Transform-based EMG feature extraction* and *Threshold-based EMG detection*. The block diagram of the complete algorithm is shown in figure 2.4.

2.1.2.1   Fourier-Transform-based EMG feature extraction

In order to use the Fourier Transform with the recorded signals, two assumptions are necessary. First, the signal and the noise are assumed to be
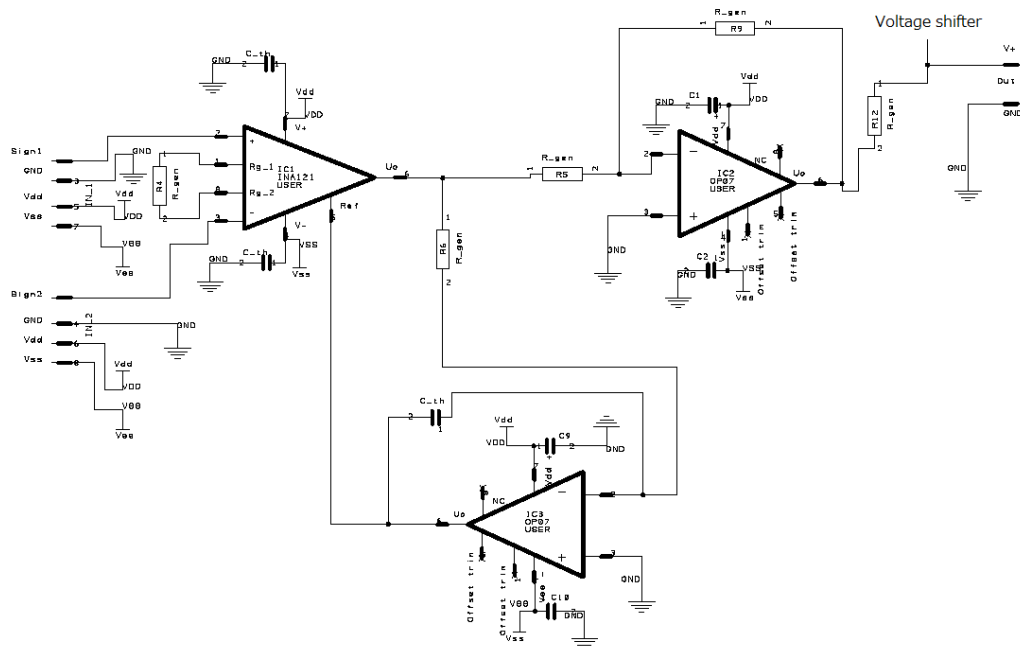
Figure 2.3: Electronic circuitry and elements of differential and amplification stages.
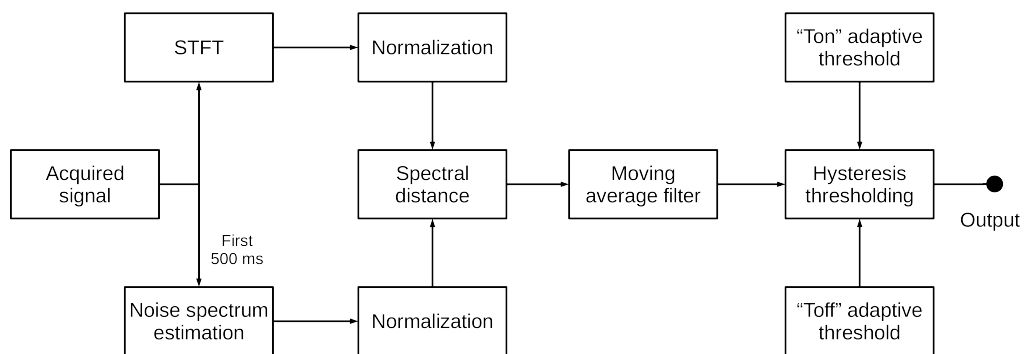
Figure 2.4: Algorithm's block diagram.

stationary inside the considered time window. Thus, it is possible to apply the Fourier Transform considering signal segments of a certain length. In other words, the Short Time Fourier Transform has been applied using a time window of 200 ms. Second, it is assumed that inside the recorded signal it is possible to identify a period of complete absence of EMG signal. This epoch will be used to estimate the initial noise power spectrum signature. This reference spectrum will then be compared with other spectra computed from the recorded signal in order to obtain a measure of dissimilarity with the estimated noise. In particular, only a part of the frequency spectrum has been considered: from 20 Hz to 500 Hz; because, according to [57], this is the characterizing part for EMG signals. Moreover, the 50 Hz component has been rejected from the estimated spectrum because it usually represents the highest contribute to the noise power in the described acquisition system.

The initial noise power spectrum signature, N_k, is estimated considering the first 0.5 s of the sampled and recorded signal, z_t . According to the experiment setup, this epoch will be free from EMG signal. N_k is computed as follows:

$$N_k = \frac{Z_k}{\|Z_k\|}$$

Where Z_k is the mean power spectrum of z_t estimated using the STFT, and $\| \cdot \|$ is the Euclidean norm. Then the Short Time Fourier Transform has been applied to the remaining sampled recorded signal s_t. In addition to providing frequency information of the signal, the STFT introduces the temporal information by applying FT to the portion of the signal contained in a sliding window [47], thus the result will be $S_{k,t}$ and it is computed as follows:

$$S_{k,t} = \sum_{m=1}^{M} s_m \cdot w_{t-m} \cdot e^{\frac{-j \cdot 2 \cdot \pi \cdot m \cdot k}{M}}$$

Where w_{t-m} is the window function and $0 \leq k \leq M-1$. The M variable was set to 200 samples in order to achieve a 200 ms window with a sampling frequency of 1 kHz. For each time instant,$S_{k,t}$ is then normalized using the

Euclidean norm $\| \cdot \|$ as for the noise power spectrum signature:

$$\hat{S}_{k,t} = \frac{S_{k,t}}{\|S_{k,t}\|}$$

The results of this first part are the initial noise power spectrum signature N_k and the normalized power spectrum for each considered window of the sampled signal $\hat{S}_{k,t}$.

2.1.2.2 Threshold-based EMG detection

Once the features to be compared are extracted, a measure of dissimilarity between the estimated noise and the part of signal under analysis is needed. Therefore, the previous results are used in order to distinguish between EMG activation and noise. The spectral distance (SD) [48] defined as the Euclidean distance, E_t, between $\hat{S}_{k,t}$ and N_k is computed as follows:

$$E_t = \|\hat{S}_{k,t} - N_k\|$$

More information about the SD and its use in image processing can be found in [48]. Finally, E_t is filtered with a moving average filter characterized by a window of 50ms. This simple smoothing helps to reduce the fluctuations of E_t during the EMG burst, and it improves the stability of the output.

To detect EMG activation, the variable E_t is compared with a threshold value T_{on}. In case the value is higher than the threshold value T_{on}, the onset of muscle activation is reported. The numerical value of the parameter T_{on} is easy to calibrate because the value of E_t has a maximum. In fact, E_t is the Euclidean distance between two L2-normalized vectors. The result of the normalization will be two vectors with unit L2 norm. Moreover, the initial vectors $\hat{S}_{k,t}$ and N_k represent power spectra, thus they only have positive components. This results in the fact that the two normalized vectors lay on the positive part of the hyper-sphere with radius equal to 1, which represents the multi-dimensional space of the normalized power spectrum vectors. Therefore, the maximum angular distance between the two vectors will be

$\pi/2$, and the maximum value that the Euclidean distance between the two normalized vectors could assume will be $\sqrt{2}$.

The value of the threshold T_{on} is referred to an adaptive threshold through a multiplicative coefficient as follows:

$$T_{on} = ON_{coefficient} \cdot T_{adaptive}$$

The initial value of $T_{adaptive}$ is set to the mean value of the Euclidean distance between N_k and the normalized power spectra computed inside z_t. Then, the value of $T_{adaptive}$ is dynamically updated during the running phase of the algorithm. Whenever the considered frame is classified as noise, the corresponding E_t is averaged with the current threshold value through a weighting factor ρ as follows:

$$T_{adaptivenew} = E_t \cdot \rho + T_{adaptive} \cdot (1 - \rho)$$

In order to deal with the imperfect stationarity of the noise, the noise power spectrum signature is updated during the running as follows:

$$N_k = \hat{S}_{k,t} \cdot \rho + N_k \cdot (1 - \rho)$$

As far as the EMG offset detection is concerned, a second threshold T_{off} is used. As in the case of T_{on}, this threshold is referred to $T_{adaptive}$ through a multiplicative coefficient as follows:

$$T_{off} = OFF_{coefficient} \cdot T_{adaptive}$$

The EMG offset is detected when the variable E_t drops under T_{off}.

The aim of the described hysteresis threshold method is to improve the robustness of E_t to fluctuations if compared with a simpler single threshold approach.

$ON_{coefficient}$ and $OFF_{coefficient}$ are determined empirically, and they are not critical for the algorithm performance.

2.1.3 Experimental Validation

2.1.3.1 EMG signal acquisition

Five young subjects participated in the study (1 female and 4 male, height $1.73 \pm 0.09m$, weight $68 \pm 12kg$, age 34 ± 7 years). All subjects are physically active (they report performing various types of routine exercise at least two days per week). Subjects' characteristics are given in Table 2.1. The experimental procedure is in accordance with the Helsinki Declaration of 2008. Each subject was asked to sit on a chair without backrest and armrest in a comfortable, upright position with hips, knees and ankles at 90 degrees. Knee extension force has been measured using a force gauge attached around subjects' right ankle. EMG activation of right quadriceps muscle group was assessed through surface contactless EMG electromyography (see *2.1.1*). Signals acquired using EMG electrodes were synchronized with those acquired using force gauge. The sampling frequency of the acquisition system was set to 1000 Hz. Visual feedback was provided to each subject. The purpose of measuring the force of contraction is to assess the ability of the algorithm to detect EMG onset and offset during different levels of generated muscle force. Experimental setup is shown in Figure 2.5.

Each subject was asked to pull the force gauge three times using 100% of maximal voluntary contraction (MVC). For each, the subject maximal value out of the three trials was used to determine the MVC level. Subsequently, the subject was asked to pull the force gauge 4 times: once using 100% of MVC, once using 60% of MVC, once using 30% of MVC, and finally once using 10% of MVC; he or she was also asked to maintain those contraction levels for around 5 s. During the acquisition, each subject was provided with a visual feedback of the force gauge output in order to maintain the force level during the recording as constant as possible. To avoid the occurrence of muscle fatigue, a rest period of five minutes between experimental trials was given to each subject as in [49]. Each subject performed the experiment twice wearing two different types of fabric between his or her skin and the

Visual feedback of the achieved percentage of MVC

Contactless EMG electrodes

Force gauge
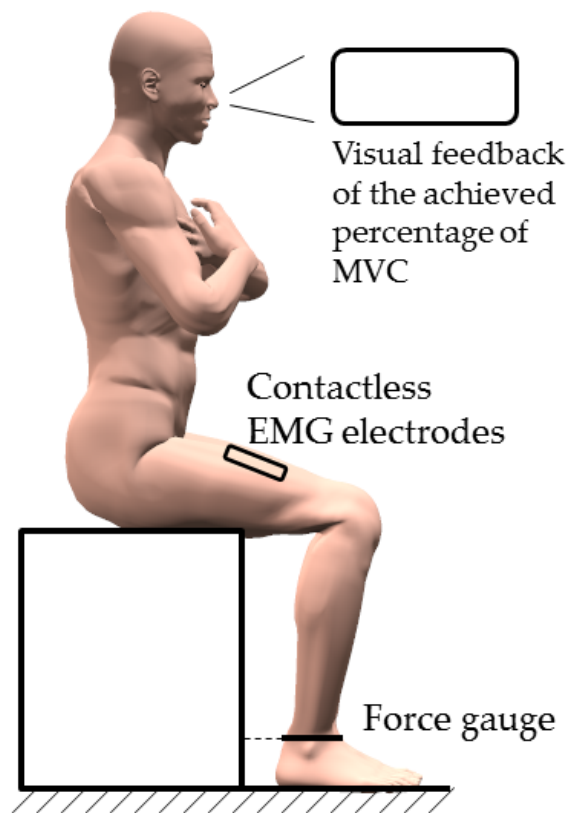
Figure 2.5: Experimental setup.

capacitive EMG electrode. The relevant characteristics of the fabrics are given in Table 2.2.

Each subject was also requested to perform the contractions following a 3-epochs template: a first part of at least 2 seconds of muscle relaxation, a middle part corresponding to the muscle contraction, and a last part of relaxation of at least 2 seconds. If a recording did not respect the defined template, it was discarded.

	Gender [M/F]	Height [m]	Weight [kg]	Age
Subject 1	F	1.62	50	33
Subject 2	M	1.75	67	24
Subject 3	M	1.69	65	33
Subject 4	M	1.86	77	41
Subject 5	M	1.71	82	39

Table 2.1: Subjects' characteristics.

	Composition	Thickness [mm]
Fabric 1	100% Cotton	1.20
Fabric 2	98% Cotton, 2% Elastin	0.60

Table 2.2: Fabrics' characteristics.

2.1.3.2 Experimental data processing

Data acquired using the system described in *2.1.1* were saved in the acquisition system and processed offline. EMG data processing was conducted by software written in MATLAB which executes the algorithm described in *2.1.2*. After the acquisition, the recorded EMG signals have been visually analyzed by an expert with the aim of creating a gold standard for the onset and the offset instants. Then, the reference has been compared with the output of the algorithm described in *2.1.2* in order to evaluate the latency between

the automatic onset/offset detection and the expert onset/offset detection. The latencies have been computed as follows:

$$\tau = |t_{goldstandard} - t_{detected}|$$

Results have been divided with respect to force level and type of fabric used during the acquisition. As in [26], [53], [54], [55] and in [56], the considered performance metrics are the mean value and the standard deviation of the latency. In order to evaluate the quality of the signal under analysis, the signal-to-noise ratio has also been estimated for each dataset. The estimation has been done by classifying each instant of the recorded signal in either signal or noise by means of the gold standard created by the expert. The results are two vectors containing the amplitudes corresponding to each instant classified as signal, S_{amp}, and the amplitudes corresponding to each instant classified as noise, N_{amp}. The signal-to-noise-ratio is estimated as follows:

$$SNR = 10 \cdot log_{10} \frac{\|S_{amp}\|}{\|N_{amp}\|}$$

Whenever the algorithm missed to detect an onset or an offset, we considered this output as an error. The percentage of error grouped for each category is represented in Table 2.4.

2.2 Results

The aim of this section is to evaluate the performance of the algorithm with data acquired in different measurement conditions. In fact, data are categorized according to the force level and the type of textile placed in between the sensor and the skin. Both variables affect the SNR of the signal and they have the purpose of simulating part of the possible measurement conditions that could affect our system. Table 2.3 collect the mean value and the standard deviation of the latencies of detection. The standard deviations are considerably high if compared to the relative mean value. This fact reflects the high variability of the single signals inside each measurement

conditions. The reason has to be researched in the nature of the acquisition system: it is sensitive to sensor positioning, pressure with the skin, humidity of the textile, property of the skin, and other subject-related factors. Nevertheless, the results summarized in Table 2.3 are not consistently different from results reported in other works, such as in [26], [53], [54], [55] and in [56]. In fact, it has been possible to achieve a value of mean latency as low as 37ms in the case of force level of 30% MVC. Furthermore, the worst performance, which has been recorded in the case of force level of 60% MVC, is characterized by a mean latency of 489ms. As far as EMG detection is concerned, some points need to be focused when different detection methods are compared. Firstly, there is no standard definition of the latency metric. For instance, in [26] the latency's formula is not reported, but from the method's description and the nature of the results it is possible to assume that the following was used:

$$\tau = t_{goldstandard} - t_{detected}$$

Conversely, [54] uses the same latency metrics definition that has been used in the present work. Obviously, it is not possible to quantitatively compare results from different metrics. Secondly, the great part of the analyzed literature uses simulated data. In order to achieve a meaningful comparison, different methods have to be applied on the same dataset.

Another confirmation about the high variability of the dataset comes from Table 2.5, which reports the standard deviation of the estimated SNR for each measuring condition. If the values of the SNR's standard deviation are compared with the respective SNR's mean value, it is possible to understand the unevenness of the recorded signals. Table 2.4 reports the percentage of error for each measuring condition.

Figure 2.6 shows a representative raw EMG signal acquired during a 30% MVC contraction, the EMG features were extracted using Fourier-Transform-based algorithm and the corresponding adaptive thresholds T_{on} and T_{off} are shown. The figure also indicates the onset and offset detection.
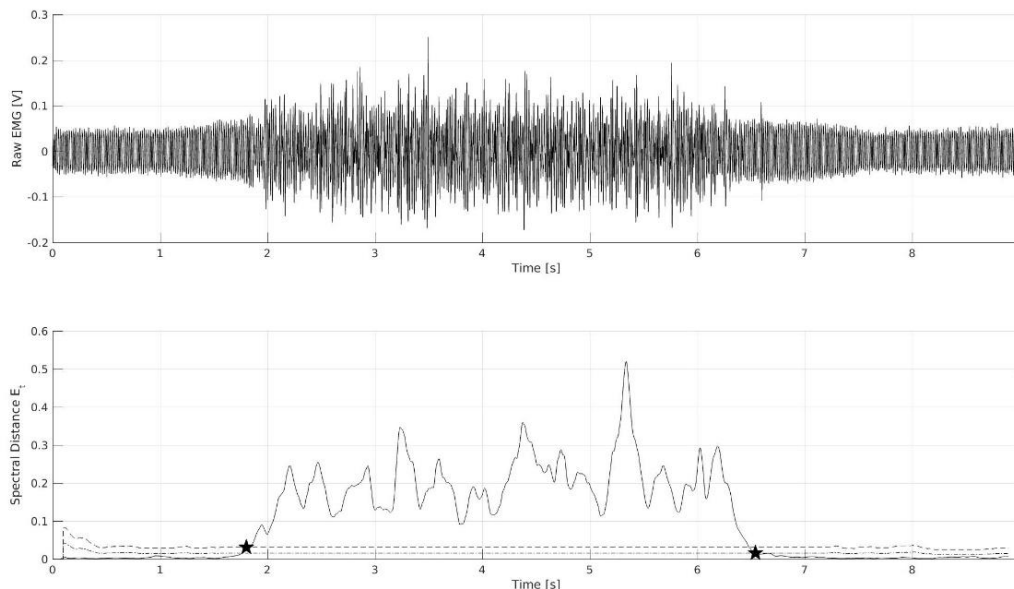
Figure 2.6: Top: Raw EMG signal acquired with contactless EMG electrodes during a 30% MVC contraction. Bottom: Euclidean distance E_t in solid line, T_{on} in dashed line (upper) and T_{off} in dash-dotted line (lower). The first star and the second star indicate the onset detection and the offset detection, respectively.

Force level	Fabric "1"		Fabric "2"	
	ON	OFF	ON	OFF
100% MVC	0.0490 ± 0.0993	0.1053 ± 0.1112	0.0886 ± 0.1242	0.2214 ± 0.1892
60% MVC	0.0414 ± 0.0673	0.1275 ± 0.1719	0.0438 ± 0.1071	0.1336 ± 0.1615
30% MVC	0.0234 ± 0.0408	0.0865 ± 0.1785	0.0652 ± 0.1335	0.1083 ± 0.1712
10% MVC	0.0424 ± 0.0555	0.1287 ± 0.2700	0.0616 ± 0.0972	0.1218 ± 0.1728

Table 2.3: Latencies' mean value and standard deviation expressed in seconds.

Force level	Fabric "1"	Fabric "2"
100% MVC	0.00	0.00
60% MVC	0.00	16.67
30% MVC	0.00	25.00
10% MVC	0.00	0.00

Table 2.4: Errors expressed in percentage over the relative dataset.

Force level	Fabric "1"	Fabric "2"
100% MVC	8.16 ± 6.83	7.06 ± 6.92
60% MVC	6.60 ± 6.94	2.25 ± 4.03
30% MVC	3.71 ± 5.19	1.62 ± 3.33
10% MVC	5.15 ± 6.22	2.06 ± 3.50

Table 2.5: SNRs' mean value and standard deviation expressed in decibel.

2.3 Discussion

A new method for processing EMG signals acquired using contactless capacitive sensors has been proposed. As explained in [26], the detection of EMG onset and offset provides important information, but it is usually suitable only to a laboratory environment with the supervision of an expert. In particular, electrodes placement, skin preparation and many other factors can influence the reliability of many algorithms existing in literature. The developed method wants to deal with these factors that usually are not constant over time.

The proposed algorithm does not want to be a more accurate alternative, in terms of latency, to the already existing ones, but it wants to maintain comparable performance while being suitable to harsher measurement conditions. Contactless capacitive measurements provides several practical advantages in terms of sensor placement, but they are characterized by an unstable output. In particular, the amplitude of the measured EMG and its related features appear as an unreliable reference for the detection of EMG

activation because of the relatively poor and highly variable signal-to-noise ratio, as explained in *2.2* and in [12], [14].

The method was tested by acquiring and processing EMG signals from five healthy subject during isometric quadriceps muscle contractions. Knee joint force was measured to verify the entity of contractions. The EMG detection was considered correct if its onset and end timings were in accordance with the onset and end timings of the respective gold standard previously created by an experienced bioengineer. Finally, the latency between the expert detection and the algorithm detection was computed to quantify the reliability of our method.

As shown in *2.2*, the proposed offline algorithm is able to reliably detect EMG activation and its performance is comparable to other methods that have been tested with simulated signals or experimental EMG signals acquired through conventional direct contact sensors. In particular, the proposed method demonstrate robustness against the highly variable range of considered SNRs.

However, some applications, such as the control of assistive devices, require online EMG detection in non-laboratory settings; thus, the algorithm was implemented into an MCU-based acquisition system and its online application was tested in laboratory condition. The first results are promising; however, more tests in real-world settings are needed.

The novelty of the described approach lies in combining short time Fourier transform with the spectral signature coding method commonly used for image processing. This approach does not depend on amplitude characteristics of EMG signals that are subject- and location-specific and might change over time due to electrode misallocation and different skin conditions. In conclusion, the independence from the signal amplitude helps in dealing with the low and highly variable signal-to-noise ratio, which is one of the most common drawbacks of capacitive sensing technology.

Chapter 3

Conduction Velocity Estimation

As explained in *1.1*, conduction velocity (CV) is the propagation speed of action potentials through different type of fibers. In particular, the muscular fibers conduction velocity is addressed in this work. As reported in [60] and [61], CV is an important physiological parameter. From CV, it is possible to asses several useful information about the investigated muscle fiber:

- Fiber membrane properties.

- Fiber contractile characteristics.

- Muscle fatigue.

- Fiber pathologies.

- Type and diameter of muscle fibers.

In particular, the last piece of information enables the estimation of another useful feature: the muscle contraction force. As explained in *1.1*, when a higher force is required from the muscle, bigger muscle fibers are recruited. They are characterized by a higher CV than smaller fibers. Thus, if any other influence factor is stable or negligible, estimating the average CV of a

muscle gives the possibility of estimating the entity of muscular contraction: the higher the required force, the higher the average CV of the muscle.

It is important to understand that the aim of this work is to estimate the CV through surface capacitive measurements and, starting from the acquired data, to verify its relationship with the entity of muscle contraction (EMC). Force level is different from EMC, and requires complex subject-specific calibrations or models because of the high inter-subject variability. In literature, other works addressed the investigation of the CV-force relationship, such as [62]; they avoided the mentioned complexity by means of a normalization with the maximum voluntary contraction (MVC). Each force level is expressed as a percentage of the subject's MVC. This helps in reducing subject-related variables and enables meaningful comparison between different acquisitions. The same approach has been followed in the present work.

CV is a useful feature in several application fields, one is medical diagnoses. As reported in [63], muscular conduction velocity is an informative parameter for the diagnosis of myogenic or neurogenic diseases. Despite its invasiveness, needle electrodes are the most common acquisition method to acquire this feature. Huppertz and co-worker claim that surface-acquired signal gives comparable results and reduce the invasiveness of the acquisition system. The proposed system aims to reduce the discomfort of the user even further as explained in *1.2*.

A second field of application is wearable devices and prostheses. Whenever a long-term EMG acquisition is required, a common surface EMG system is unsuitable. As reported in [12], surface electrodes are origin of discomfort, skin allergy and inflammation during long measurement periods. *2* illustrates how it is possible to reliably detect EMG activation with capacitive sensing, but, as far as device control is concerned, a more accurate approach is necessary. The user not only need to control the activation of the prosthesis or the wearable device, but also the intensity or speed of the movement. Thus, CV estimation through capacitive sensing could bring a solution in

this application field.

As for EMG activity detection, it is possible to investigate EMG amplitude-related features in order to estimate the entity of muscle contraction. However, the same considerations about the instability and the unreliability of amplitude-based features are valid in this case. If the application requires a long-term and unsupervised measurement, amplitude-based features are not suitable.

The estimated EMG spectrum mean frequency (MNF) could be another possible feature for the estimation of subject's force intention. Some literature's articles reports the existence of a relation between force and MNF. However, another comparable number of researches report contradictory results. Angkoon and co-workers [59] investigated on the situation and they concluded that the relation between force and MNF is strongly subject-dependent and still unclear. After some preliminary studies, it was decided not to exploit MNF to estimate subject's entity of muscle contraction in the present research.

The aim of the following work is to design a capacitive acquisition system composed of sensors, hardware and software that is able to estimate conduction velocity even with clothes placed in between sensors and subject's skin. This wants to cope with the described issues and with user discomfort during long-term acquisitions.

3.1   Methods

3.1.1   Acquisition system

3.1.1.1   Array of capacitive-sensing electrodes

The proposed design is a capacitive-sensing electrode array, which can be composed of several electrode units organized in different patterns. A five-electrode one-dimensional array prototype has been chosen as a first implementation, but any configuration could be designed accordingly to re-
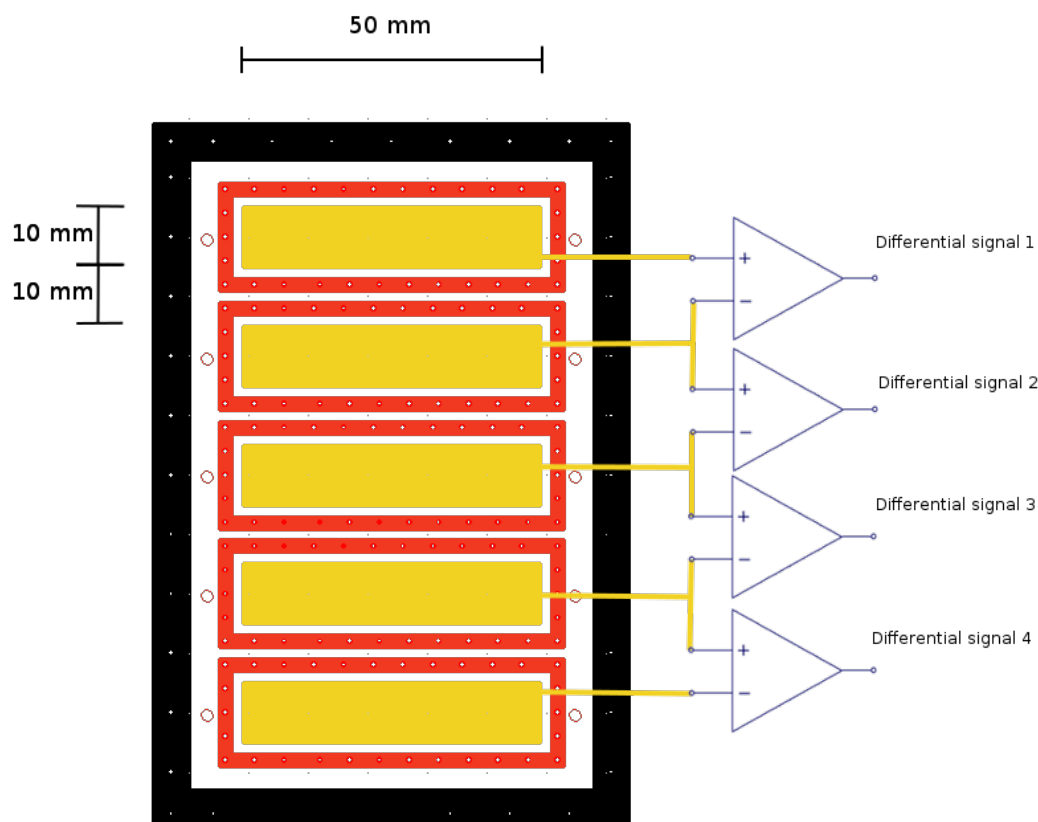
Figure 3.1: Representation of electrodes array with differential signals generation. Black surface represents the ground shield. Red surfaces represent the driven shields. Yellow surfaces represent the electrodes' sensing area.

quirements. A representation of the designed electrode array can be seen in figure 3.1. In order to deal with the common mode noise, each acquired signal consists of the difference between two consecutive electrode. Thus, a five-electrode array will be able to acquire four single-differential signal. The acquisition does not need any particular preparation of the skin, nor any kind of conductive gel. They can be used directly on the clothes of the subject. Thus, a capacitive-sensing EMG system could even be embedded in a consumer applications.

In terms of signal acquisition, capacitive-sensing electrodes are different from contact-based ones because they demand more precautions.
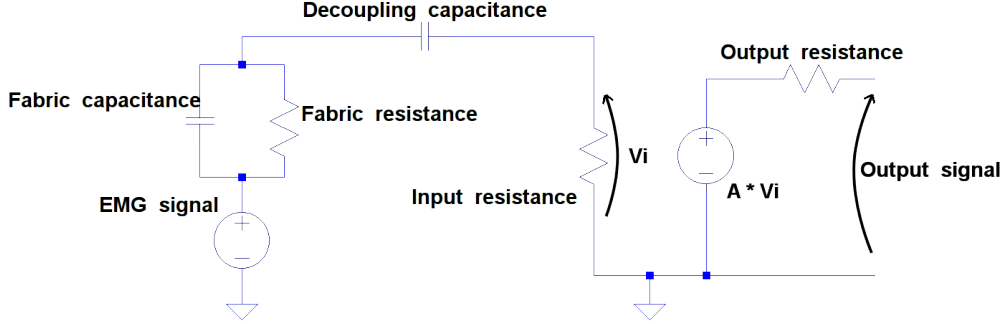
Figure 3.2: Simplified electrical model of electrode and input stage system.

The first precaution: dimensions and mutual distances of the electrodes is important in order to achieve a good Signal-to-Noise-Ratio (SNR). The dimension of the sensing area is directly related to the value of capacitance that characterize the capacitive coupling between skin and electrode. Thus, the amplitude of the detected signal is influenced by electrode's physical dimensions. It is possible to model the skin-electrode system as a parallel-plate capacitor, see figure 3.2. The capacitance value can be computed with the classical parallel-plate-capacitor formula:

$$C = \frac{\varepsilon \cdot A}{d}$$

Where ε is the dielectric constant, A is the sensing area and d is the distance in between the skin and the electrode. However, fabrics are not perfect insulators, thus the system is not dealing with perfect capacitors. Each textile is characterized by a resistivity value and its resistance can be computed with the known resistance formula:

$$R = \frac{\rho \cdot d}{A}$$

Where ρ is the resistivity of the material, A is the sensing area and d is the distance in between the skin and the electrode. The two effects combine in a parallel of an ideal resistor and an ideal capacitor. Depending on the material, the impedance due to one element can be considerably higher than

the other that can be neglected. Hence, it is not possible to plan to draw any DC current from the subject's body. It will result in a unreliable system, strongly dependent on which material is placed under the electrodes. As shown in figure 3.2, the proposed system includes a decoupling capacitor on the input line, thus do not rely on biasing current drawn from the electrodes.

The second precaution regards shielding. A driven shield is required for each electrode due to their working principle. A small amount of charge will accumulate on each electrode, and a shielding technique is necessary in order to prevent leakages of this charge. Driving each shield at the same potential of the respective electrode will considerably reduce the leakage current. Each shield, which is driven by the electronics, surrounds the respective electrode. The electrode, is exposed just in the bottom face; it consists of a gold-plated copper area. Gold improves the conductivity and avoid copper oxidation. One important note needs to be done on the driven shield: it has to be insulated from the sensed surface. In fact, the weak nature of the EMG signal make it susceptible to any interference. Placing the driving shield in direct contact with the skin or with the sensed cloth will impose the sensed surface at shield's electrical potential. The acquisition will result in five almost identical input signals. Figure 3.3 and figure 3.4 show the resultant differential signals without and with driven shield electrodes insulation, respectively. As far as the former is concerned, it is possible to notice that the signals acquired with inner electrodes. Conversely, signals acquired from outer electrodes are characterized by a higher energy, but a more accurate investigation reveal that they are almost identical, as shown in figure 3.5. After the correction, it is possible to observe that each signal is the delayed noisy copy of the adjacent signals, as shown in figure 3.6. Insulating the driven shield electrode can not be neglected.

An outer shield is added on the back of the array and it is connected to ground. It has the aim of reducing electrical noise coming from the environment.

The electrode array is realized on a multilayer flexible PCB. Thus, ac-
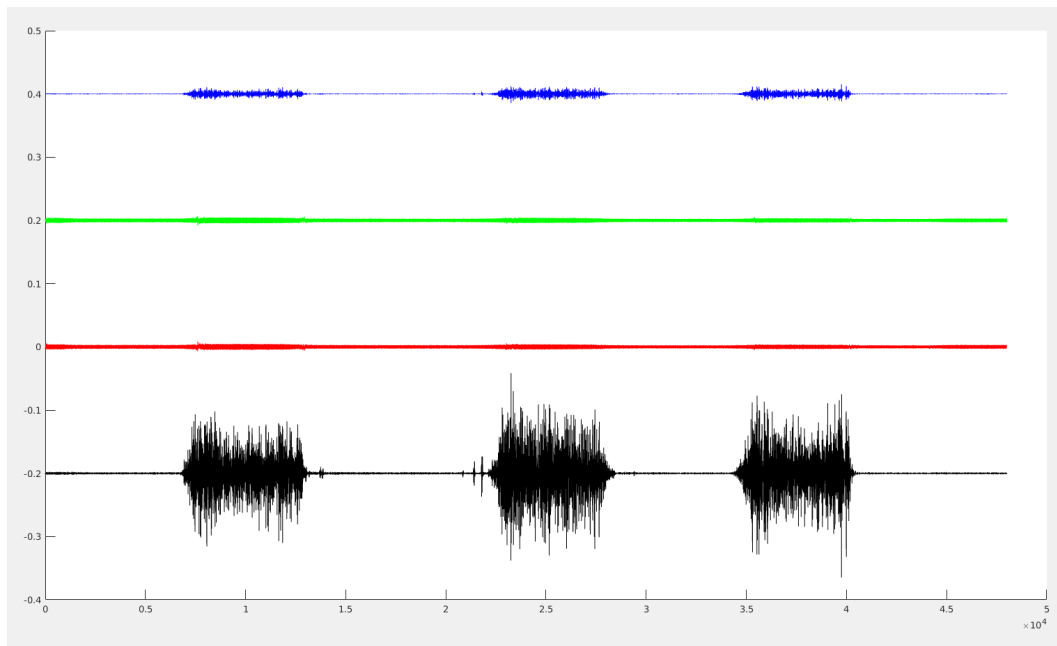
Figure 3.3: The four resultant signal from an acquisition on vastus medialis without driven shield electrode insulation
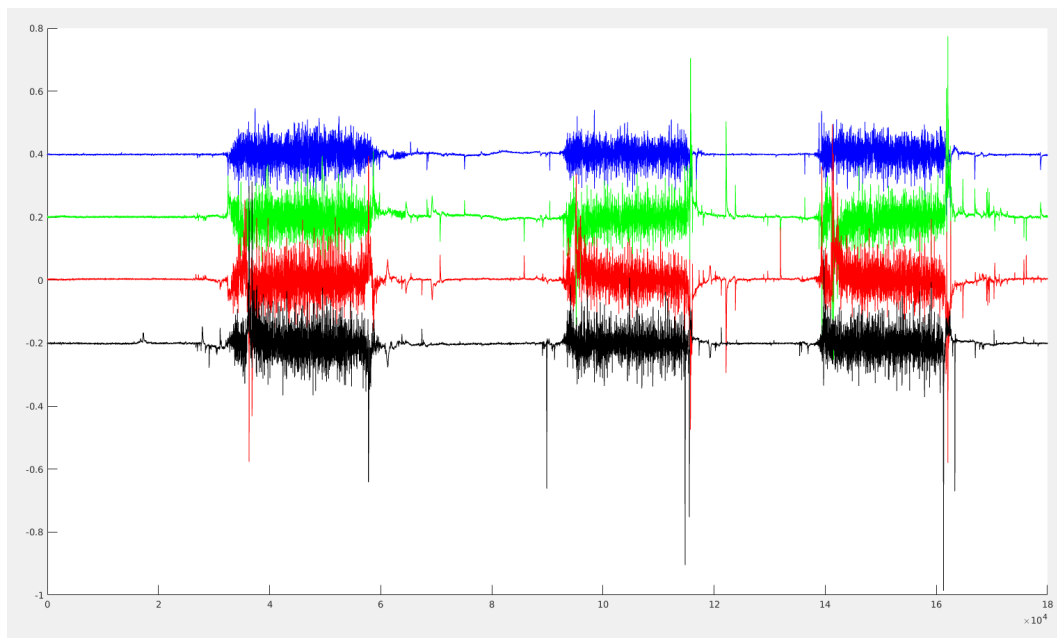
Figure 3.4: The four resultant signal from an acquisition on vastus medialis with driven shield electrode insulation
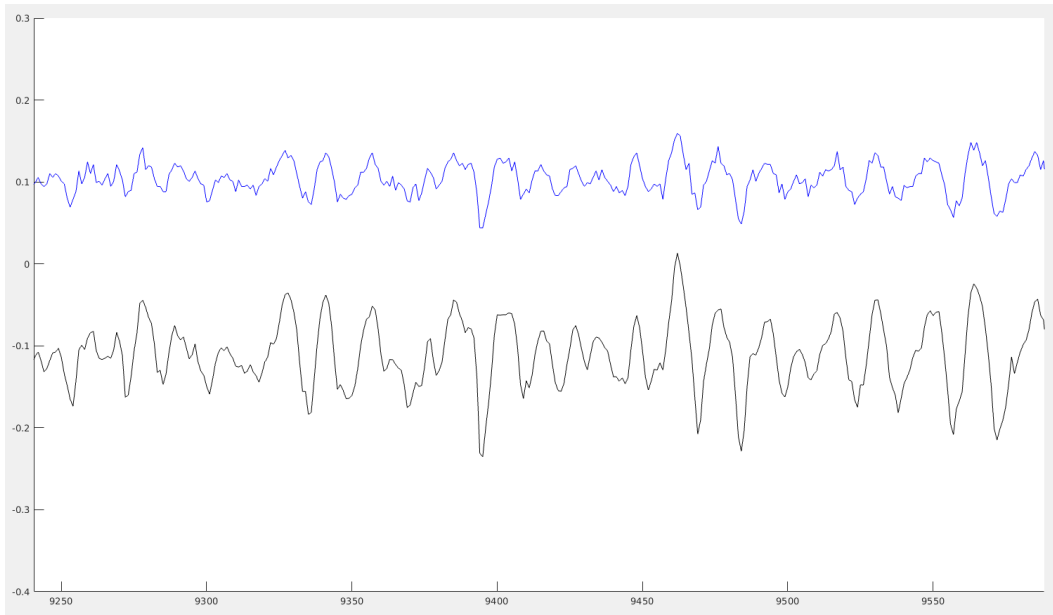
Figure 3.5: Zoom of the first signal and the last signal of acquisition represented in figure 3.3.
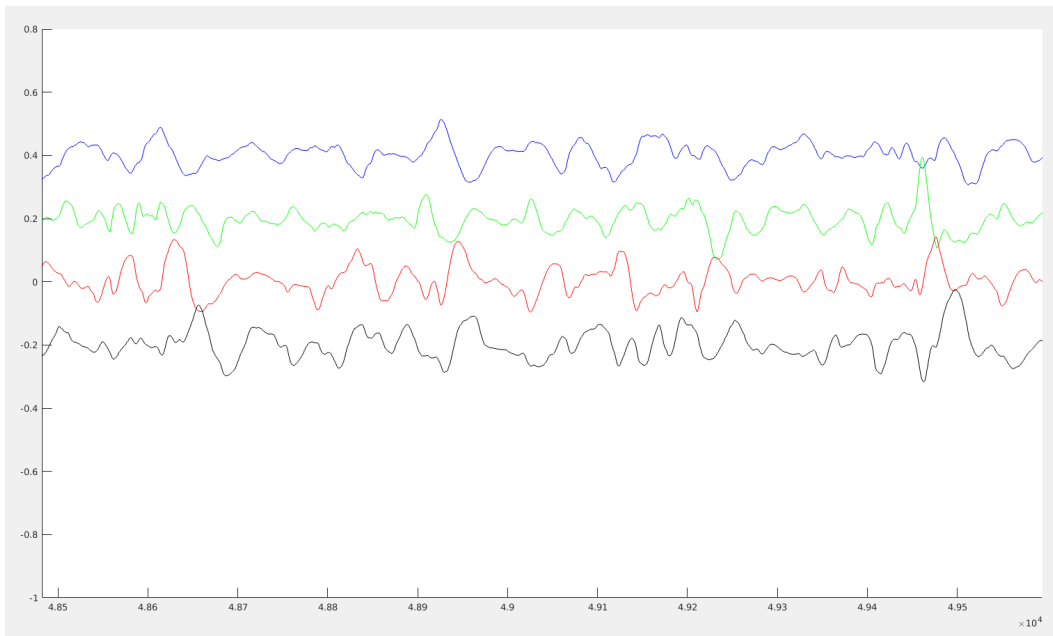
Figure 3.6: Zoom of the four resultant signals of acquisition represented in figure 3.4.

curate patterns and shapes are easy to achieve. Electrodes should not be covered by any solder mask in order to avoid any charge accumulation. Realizing electrodes as a multilayer flexible PCBs brings about important practical advantages:

- It is not necessary to engineer the production of the electrodes, because it already exist.

- Obtaining complex shape and patterns with high accuracy is easy.

- Productive costs will be comparable to a normal PCB manufacturing cost.

- Electrodes properties (mechanicals and electrical) are easy to control thanks to the high reliability of PCB manufacturing process.

- Flexible structure makes the embedding of this electrodes in wearable devices easy. They do not necessarily have to be embedded inside clothes, but the subject can wear his/her own clothes and he/she can wear the electrodes on them.

- Electronics can be miniaturized and mounted on the the electrodes themselves. SNR will be improved and system dimensions will be drastically reduced.

Some acquisitions on different muscles revealed an issue related to sensors' dimensions. The cross-talk from nearby muscles is a critical factor that needs to be addressed in order to achieve a reliable CV estimation. Dimensions shown in figure 3.1 were excessive for the major part of the investigated muscles, especially vastus medialis that was investigated in *3.1.3*. The problem was solved with a reduction of the sensing area. Figure 3.6 and figure 3.7 show an acquisition from vastus medialis before and after the described corrections, respectively. Figure 3.8 shows the final version of the electrode array. Resizing of the electrodes has been done by insulating a part of the sensing area with polyimide tape. Since data acquisition has been done with
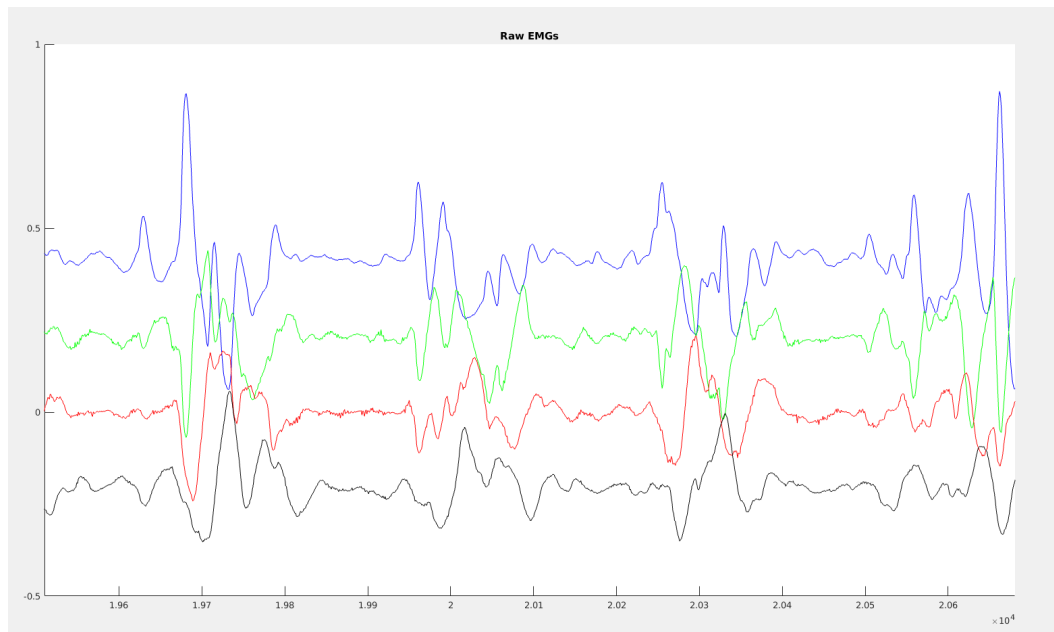
Figure 3.7: Zoom of the four resultant signals of an acquisition on vastus medialis after electrodes' dimension resize.

cotton fabric in between electrodes and subjects' skin, polyimide offers a suitable impedance to insulate electrodes if compared to cotton's impedance.

3.1.1.2   Electronics

Acquiring EMG signals through capacitive-sensing electrodes brings about two main difficulties. The first one is the high impedance of the electrodes. In between the skin (conductor) and the sensor (conductor) there is a sheet of cloth (insulator); ideally, this configuration acts as a capacitor. This brings about that it is not possible to draw any DC current from this path. The second issue regards the noise. EMG signal is very low in amplitude and, when electronics deals with electric signal in the range of microvolts, a particular attention on interferences and electronic noise has to be taken into account. The output of the electronics is a differential signal taken from two adjacent electrodes (electrode A and electrode B). This is of critical importance in dealing with common mode noise rejection. The different part of the circuit
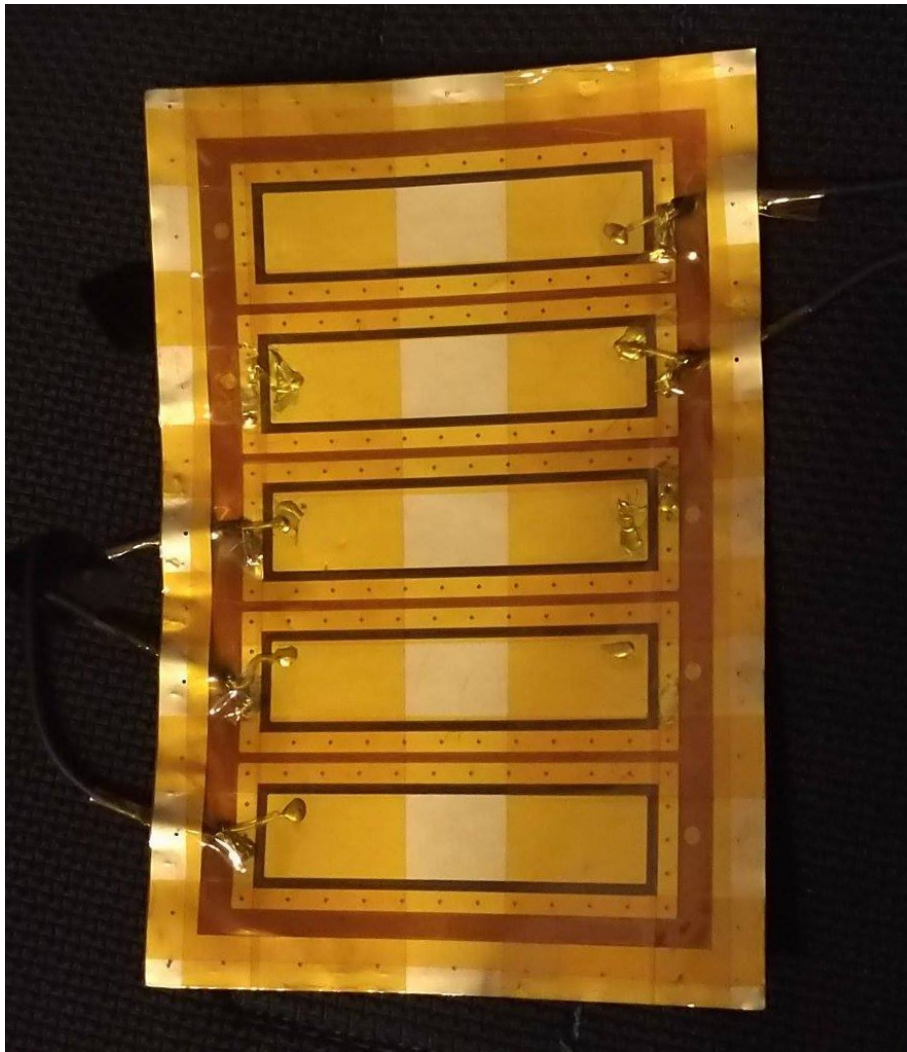
Figure 3.8: Latest version of the capacitive-sensing electrodes array. The new sensing area is 15 mm wide.
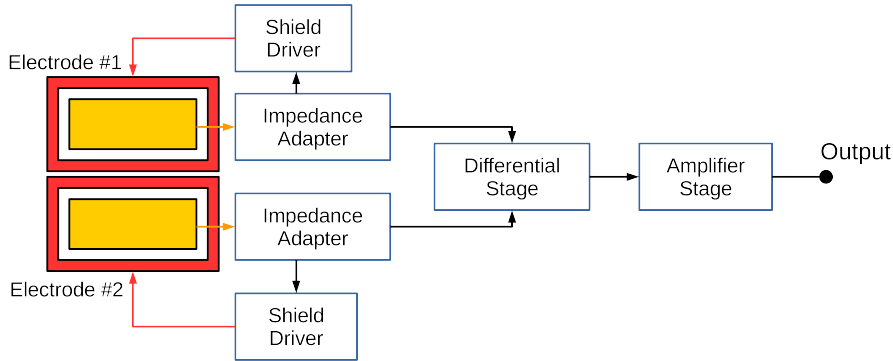
Figure 3.9: Electronic system's block diagram.

are described in the following paragraphs. More detail about PCBs layout can be found in *Appendix A*. A schematic overview of the complete electronic system is shown in figure 3.9.

Impedance adapter   Impedance adapter acts as the input interface. As mentioned above, it should be characterized by a high input impedance in order not to spoil the weak input signal. Moreover, two copies of this circuit are present in the design because the output signal needs to be the result of a differential acquisition. The schematic of this first part is shown in figure 3.10 and figure 3.11.

Capacitors C3 and C10 are decoupling capacitors. They have the aim of blocking any DC signal and of keeping the following stages away from saturating. In fact, since the configuration skin-cloth-electrode is not a perfect capacitor, its characteristics could change over time because of subject's movement. Thus, several types of motion artifact could be injected into the system. A decoupling capacitor is an easy and inexpensive way to deal with low-frequency motion artifacts.

Operational amplifiers do require a DC current path for their input stage in order to bias their input transistors. Even if some manufacturers developed operational amplifiers characterized by a very low DC bias current, a DC current path is needed. This is obtained by using high value resistors: R1
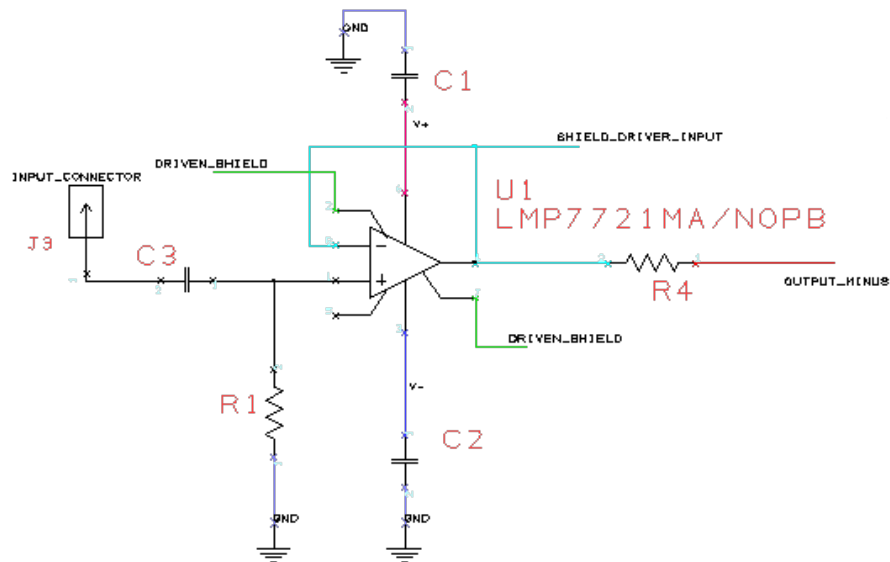
Figure 3.10: Impedance adapter for the signal taken from electrode A.
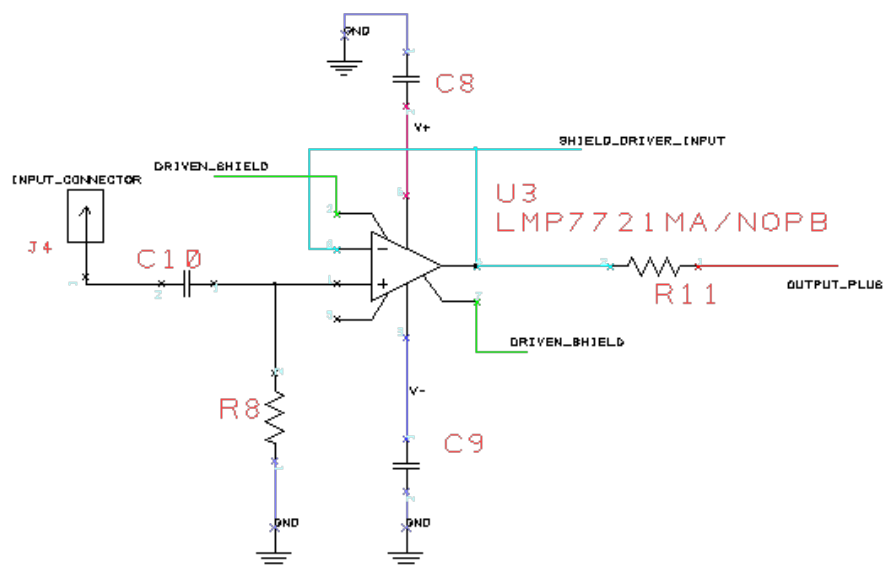
Figure 3.11: Impedance adapter for the signal taken from electrode B.

and R8. High value resistors can provide a suitable DC biasing current and preserve the signal at the same time.

LMP7721 was chosen as operational amplifier for the impedance adapter. It requires an extremely low DC-bias current and it provides dedicated pin for input's shielding. These features make the LMP7721 a suitable device for EMG signal acquisition. As mentioned above, noise is an important issue to deal with when low-amplitude signals are acquired. In order to reduce both noise due to electronics and common mode noise, a voltage-buffer configuration was implemented. The signal is amplified only after being subtracted from the adjacent signal.

Resistors R4 and R11 provides the LMP7721 operational amplifiers with a short-circuit protection.

More details about LMP7721 and its applications can be found in [64] and [65].

Shield driver The second part of the first stage, shown in figure 3.12 and figure 3.13, involves the LMP7715: a low noise and low voltage supply operational amplifier. This device has the purpose of driving the shield of the electrode. Shielding techniques are very important when low current input signals are involved: any noise from the environment could spoil the signal. In this case the shielding is done by creating a copy of the signal that surrounds the input conductors. The voltage difference between the input conductors and the surrounding volume will be close to zero, thus the leakage current will be very low. Input conductors includes electrodes, connectors and PCB paths.

Unfortunately, the shield is characterized by a considerably high capacitive load, thus, as mentioned in [64], it is recommended to drive it with a suitable driver, such as the LMP7715. This amplifier picks up the signal from LMP7721's V- pin and it drives the shield.

Resistors R5 and R12 have a critical importance in the circuit stability. As explained in [64], they create the correct interface conditions between
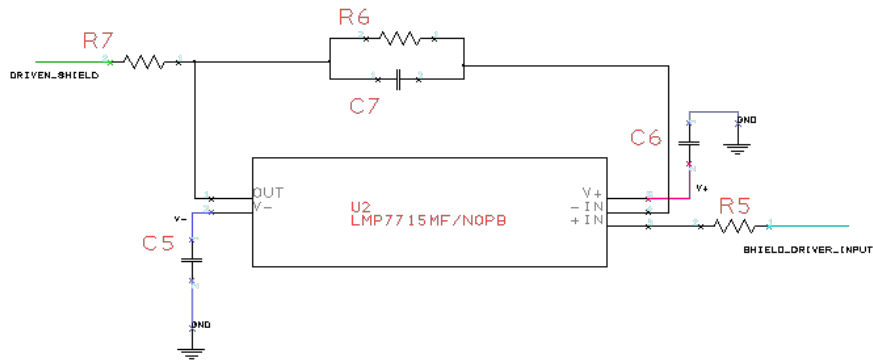
Figure 3.12: Shield driver for the signal taken from electrode A.
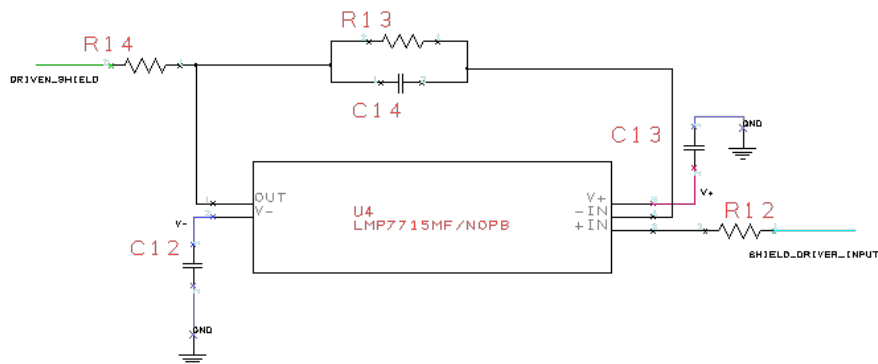
Figure 3.13: Shield driver for the signal taken from electrode B.
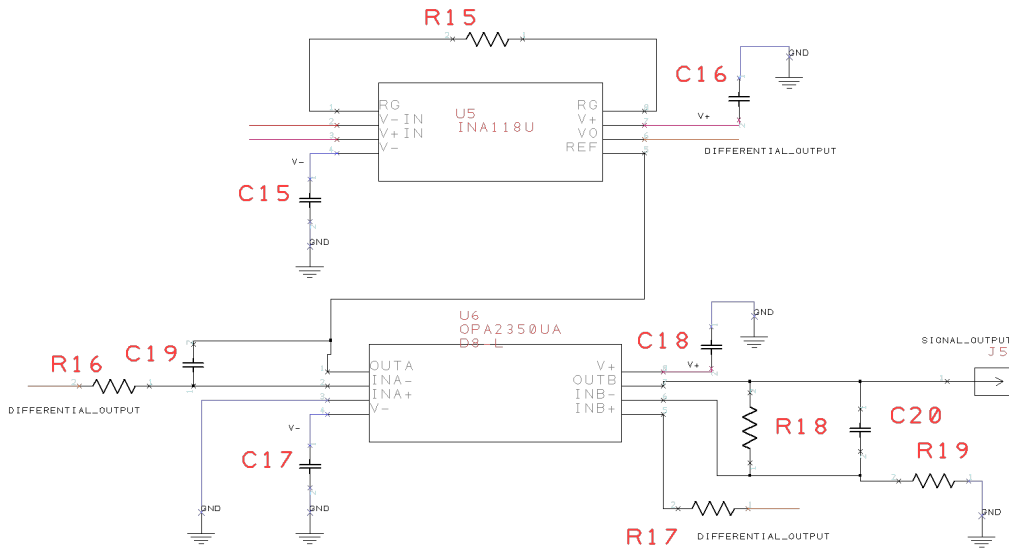
Figure 3.14: Differential stage and amplifier stage.

LMP7721 and LMP7715 in order to deal with parasitic effects from both devices.

The couples R6-C7 and R13-C14 creates a low pass filter and they control the shield driver bandwidth. They have the purpose of preventing the shield driver from peaking due to high frequency signals and keeping the system stable. The bandwidth was set to 500Hz, according to [57], this value correspond to a good choice of upper limit for EMG bandwidth.

Resistors R7 and R14 limit the current that is drawn from LMP7715's output. They provide a short-circuit protection and they avoid the device from peaking due to the shield's high capacitive load.

Capacitors C5, C6, C12, C13 provides power-supply noise reduction.

Differential stage   Once the two signals have been acquired, they serve as input for the differential stage. As mentioned above, this stage has critical importance in common-mode noise rejection (CMR). The low-power high-CMR instrumentation amplifier INA118 was chosen for this purpose. The circuit is shown in figure 3.14.

Resistor R15 determines the gain of the stage that was set to 51.

In order to deal with motion artifacts and low-frequency noise outside EMG bandwidth, an AC-coupling configuration was chosen. The output of the instrumentation amplifier serve as input for another operational amplifier, its output determines the reference of the INA118. The low-supply-voltage low-noise OPA2350 was chosen for this purpose.

The couple C19 and R16 brings about a low-pass filter effect that translates into a high-pass filter effect for INA118. The high-pass cutoff frequency was set to 50Hz. As shown in [66], this reduces the bandwidth of INA118 and it helps in dealing with low-frequency noise.

Capacitors C15, C16, C18 and C19 provides power-supply noise reduction.

Amplifier stage   The final stage has the purpose of providing the acquired signal with the correct amplitude in order to be suitable for digital acquisition. As shown in figure 3.14, the second OPA2350 present in the same package of the device used in the previous section was used. The amplifier was configured as an active low-pass filter with a cutoff frequency of 500Hz, as suggested in [57].

Resistors R18 and capacitor C20 determine the low-pass filter effect.

Resistors R18 and R19 determine the gain of the amplifier, that was chosen to be 11. The total pass-band gain of the circuitry is then 561.

Power supply   The purpose of the system is to be used in wearable devices, thus it is necessary to devise a convenient power supply system. The portability is an important feature even in this first prototype, because it will bring about the possibility of real case use tests. As shown in figure 3.15, a CR2032-battery-based power supply was chosen.

Diodes U7 and U8 serves as protection in case of polarity inversion of the batteries.

The switch U9 turns ON and OFF the system.

Ultimately, in order to improve the robustness of the output to external interferences, a right-leg-electrode has been included and connected to
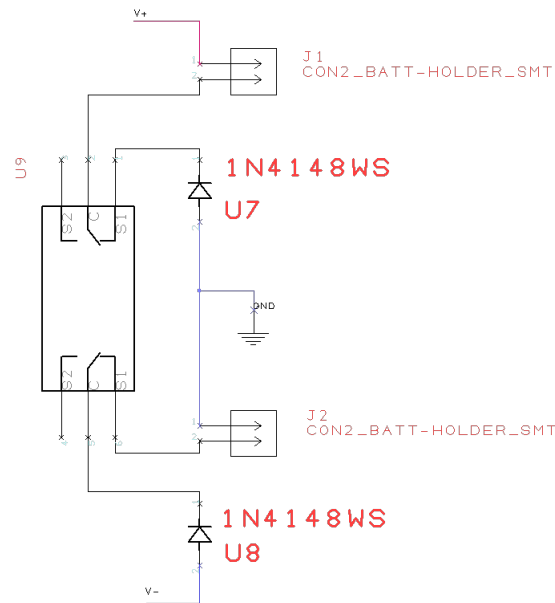
Figure 3.15: Power supply.

ground.

A picture of the complete hardware system is shown in figure 3.16.

3.1.2 Conduction velocity estimation algorithm

The aim of the algorithm is to reliably estimate conduction velocity from datasets acquired through the acquisition system described *3.1.1*. This first implementation does not aim to deal with online applications, but data are analyzed offline after being acquired and saved into a PC. The purpose is to obtain the estimation of CV on data recorded during a constant-force isometric contraction.

Ideally, the algorithm should deal with four signals that are four identical copies but translated in time. This translation is the time that action potentials need to travel from an electrode's sensing area to the following one. If the distance and the traveling time are known, it is possible to establish the speed of the traveling signal. Unfortunately, this ideal world does not match
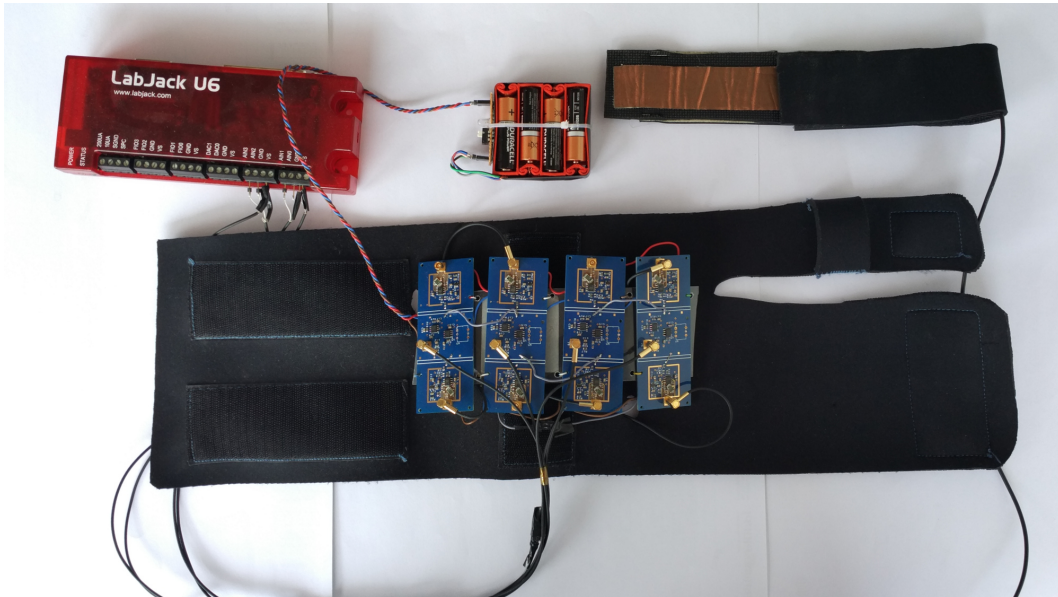
Figure 3.16: Picture of the complete hardware system.

the real condition. In fact the considered signal is a combination of several action potentials traveling on different muscle fibers. Thus, this algorithm does not want to estimate the CV of a single fiber, but the average CV which characterize the area sensed by the electrodes. As explained in [67], the ideal situation differs from the real for several factors:

- The alignment of the detection system may not coincide exactly with the conduction direction of muscle fibers. This will lead to an overestimation of the CV, because the projection of the inter-electrode distance on the muscle fibers' direction will be lower than in the case of perfect alignment.

- The positioning of the electrodes along fibers' length has a critical importance. In order to avoid an incorrect acquisition, they should not be too close to tendons. Moreover, the positioning should consider the innervation zone. Otherwise, two signals with opposite propagation direction will be acquired, as explained in [68].

- Each muscle fiber has its own CV. Thus, the estimated CV will be a
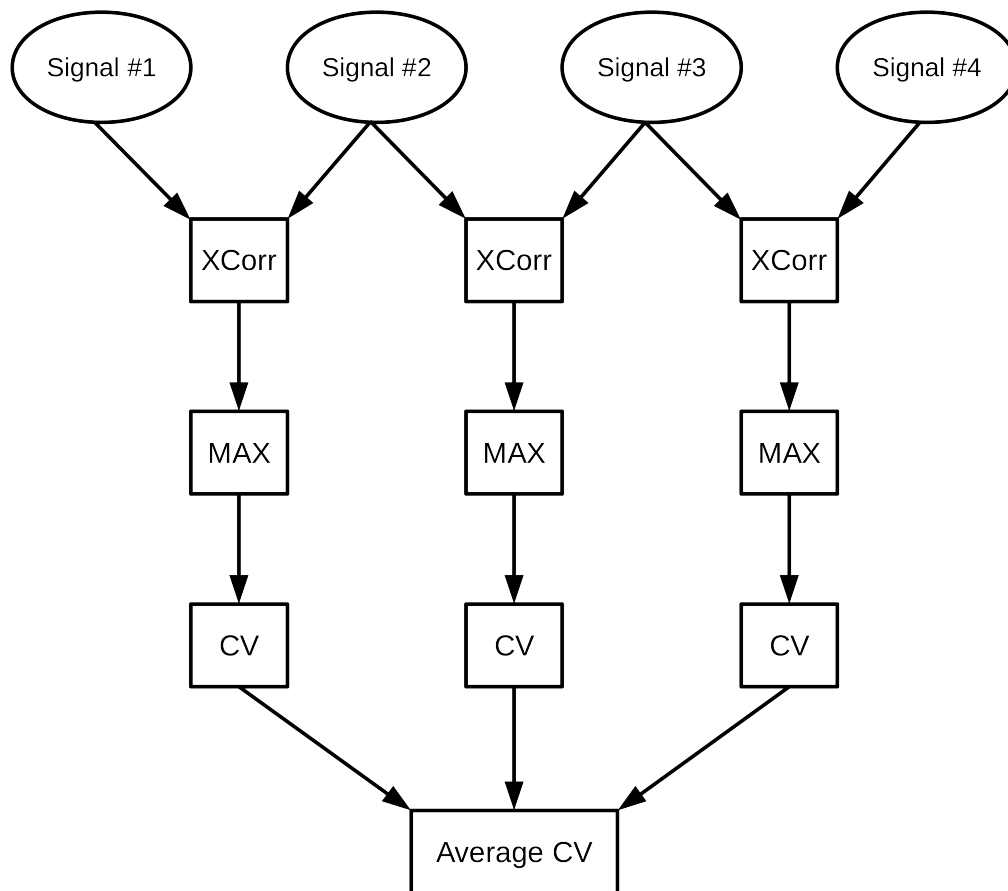
Figure 3.17: Algorithm's flow chart.

combination of the sensed muscle fibers.

- The shape of the signal will be the result of the propagation through inhomogeneous tissues and fabric. Thus, it will not be constant during the signal traveling path.

Considering the previous difficulties, an algorithm based on cross-correlation was chosen. The flow chart of the algorithm is shown in figure 3.17. The code was implemented in MATLAB version R2016a.

As pictured in the flow chart, cross-correlation is applied to each couple

of adjacent signals. The following formula was used:

$$\hat{R}_{E_1E_2}(m) = \begin{cases} \sum_{n=0}^{N-m-1} E_{1_{n+m}} \cdot E_{2_n}^* & if \quad m \geq 0, \\ \hat{R}_{E_1E_2}^*(-m) & if \quad m \leq 0. \end{cases}$$

Where E_1 is the considered part of the signal acquired from the first electrode and windowed with a 1s-wide Hamming window, E_2 is the considered part of the signal acquired from the second electrode and windowed with a 1s-wide Hamming window. Thus, the considered epochs of signals E1 and E2 are 1s wide and they are centered on the time instant under analysis. m is the time lag and N is the number of vector samples corresponding to the length of 1s of acquisition.

After computing cross-correlation, its maximum is searched inside a possible time lag span. In particular, a physiological range of conduction velocity is scanned. The lower limit is 3 m/s and the upper limit is 7 m/s. This choice was made in accordance with results from [61], [60], [62]. The considered CV range results in a feasible time lag span that goes up to 6,67ms if the designed inter-electrode distance is 20 mm. In order to find the maximum, the following relation is used:

$$\hat{R}_{E_1E_2\,MAX} = MAX\{|\hat{R}_{E_1E_2}(m)|\}$$

Once the maximum is found, the corresponding time lag value is extracted. Following [69], a parabolic interpolation on the cross-correlation function (CCF) is computed around the detected maximum. The length of the interpolation has been set to 2 ms and the interpolation factor has been set to 50. According to [69], this technique provide comparable results to spectral matching and whole interpolation on the CCF while being more computationally efficient. Then, the maximum peak of the interpolated CCF is searched and the corresponding time lag, τ_{int} is extracted. Finally, the CV is computed as the ratio between distance and time lag as follows:

$$\hat{C}V = \frac{d}{\tau_{int}}$$

Where $\hat{CV}$ is the estimated CV and d is the inter-electrode distance.

Once the CV is computed for each couple of adjacent electrodes and each time instant, non-physiological CV values are discarded. As mentioned before, a lower limit of 3 m/s and an upper limit of 7 m/s are considered. Eventually, an average value of CV on the considered dataset is computed. For each time instant the algorithm averages only the selected physiological CV values.

The output of the algorithm is the value of the average CV obtained combining the information from the complete set of the four signal during a constant-force and isometric contraction, as stated in the hypothesis.

3.1.3   Experimental setups

The devised experimental setups had the purpose of acquiring data during isometric not-fatiguing constant-force muscle contractions. As exposed in the introduction of the present chapter, CV is influenced by several factors; thus, reducing CV-influencing variable has a critical importance. Vastus medialis obliquus (VMO) was chosen to be the investigated muscle for the complete set of subjects. According to [70], VMO is characterized by a good innervation zone uniformity if different subjects are considered, and it has an excellent signal quality. Moreover, its position reduces crass-talk from other muscles because there are no adjacent muscles of comparable size. This last consideration has a critical importance when the acquisition is performed with wide-sensing-area electrodes. The experimental setups were designed following [62], and a schematic view of the whole process is shown in figure 3.18.

The first experiment aimed to investigate the reproducibility of the results over time for the same user. In the first place, the subject was asked to wear the electrodes in direct contact with the skin. He was asked to stand up with the right foot on a scale and the left foot on the ground. Then, the subject had to bend his knees and to reach a knee-joint angle of 110°. Further, he was asked to move the barycenter of the body from left to right in order
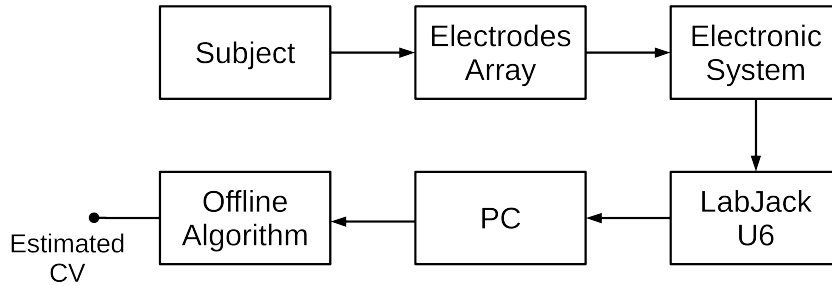
Figure 3.18: Block diagram of the experimental setup.

to increase the percentage of his weight supported with the investigated leg. The subject had a visual feedback about the supported weight through the output of the scale. The increasing in the supported weight had to follow a specific ramp:

- 5s at 25% of the weight.

- 5s at 50% of the weight.

- 5s at 75% of the weight.

- 5s at 100% of the weight.

The acquisition was repeated five times with at least fifteen minutes of rest in between two acquisition. After two hours from the end of the acquisitions, the subject was asked to repeat the same experiment with a sheet of 100% cotton fabric in between the electrode and the skin.

The second experiment aimed to investigate the reproducibility of the results between different subjects. Nine healthy people were tested, their antropometric characteristics are shown in table 3.1. Only the contacless acquisition was investigated in this second experiment due to limited subjects' availability. Each subject was asked to sat on a chair with the feet hanging down. One extremity of a belt was connected to his or her ankle and the other extremity to the force feedback system, described in *Appendix B*. The length of the belt was adjusted in order to set a knee-joint angle of 110°.

In order to acquire data from VMO, the electrodes array was placed on the right leg of the subject following the indications provided in [70]. A sheet of 100% cotton fabric was placed in between the electrodes array and the skin of the subject. The sheet was changed after each acquisition session for hygienic reasons, but the same material was used for each acquisition. Figure 3.19 shows two pictures of the second experimental setup with one of the subjects.

In both experiments, the signals coming from the acquisition system were sampled and converted to digital through a Labjack U6. This device is a configurable acquisition board; its features are summarized in table 3.2. Data were acquired through LJstreamUD, a Labview application provided by the manufacturer, and stored on a PC. Acquired data were then fed into the algorithm described in *3.1.2* and results were collected and can be consulted in the next section.

	Gender [M/F]	Height [m]	Weight [kg]	Age
Subject 1	M	1.76	95	25
Subject 2	M	1.75	67	25
Subject 3	M	1.82	80	25
Subject 4	M	1.80	66	25
Subject 5	F	1.68	60	25
Subject 6	M	1.82	85	25
Subject 7	M	1.79	80	24
Subject 8	M	1.75	71	24
Subject 9	M	1.85	90	19

Table 3.1: Subjects' characteristics.

Feature	Value
Number of analog inputs	14
Voltage input range	± 10 V
Resolution	16 bits
Input impedance	$1 G\Omega$
Typical input bias current	20nA
Sample frequency	5KHz

Table 3.2: Labjack U6's characteristics.

3.2 Results

3.2.1 First experiment

As far as the first experiment is concerned, each recording was splitted into four epochs. One epoch for each force level. Further, they were fed into the algorithm described in *3.1.2*. The output is an average CV value for each force level and each recording.

Table 3.3 reports results from acquisitions with direct contact on the skin and table 3.4 reports results from contact-less acquisitions. As performed in [62], each CV value was normalized with respect to the CV corresponding to the lowest force level during the respective acquisition. Expressing each CV value as the percentage variation from the lowest force level enable a more reliable comparison between different recordings. Table 3.5 reports normalized results from direct-contact acquisition and table 3.6 reports normalized results from contact-less acquisition.

The box plot of the complete set of CV is shown in figure 3.20 and its normalized version in figure 3.21.

Two CV influencing factors have been analyzed: the measurement method (direct-contact or contact-less acquisition) and the percentage of supported weight from the leg (related to the level of force supplied by the muscle). A two-way unbalanced ANOVA was performed on the complete set of acquired

Figure 3.19: Pictures of the second experimental setup.
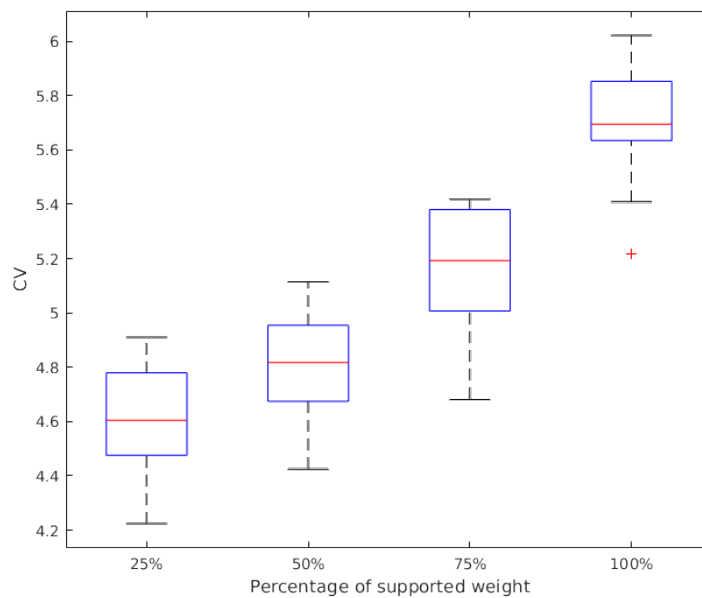
Figure 3.20: Box plot of the complete set of CVs from the first experiment.

	25% weight	50% weight	75% weight	100% weight
Rep. 1	4.22	4.67	5.15	5.68
Rep. 2	4.52	4.96	5.23	5.72
Rep. 3	4.91	4.95	5.41	5.91
Rep. 4	4.80	4.76	5.15	5.72
Rep. 5	4.78	4.95	5.35	5.85

Table 3.3: Average CV values acquired through direct contact with the skin during the first experiment. CV values are expressed in [m/s].

	25% weight	50% weight	75% weight	100% weight
Rep. 1	4.25	4.42	4.92	5.22
Rep. 2	4.48	4.75	5.01	5.41
Rep. 3	4.55	4.58	4.68	5.63
Rep. 4	4.68	4.88	5.42	5.64
Rep. 5	4.66	5.11	5.38	6.02

Table 3.4: Average CV values acquired through contact-less sensing during the first experiment. CV values are expressed in [m/s].

	25% weight	50% weight	75% weight	100% weight
Rep. 1	1.00	1.11	1.22	1.34
Rep. 2	1.00	1.10	1.16	1.26
Rep. 3	1.00	1.01	1.10	1.20
Rep. 4	1.00	0.99	1.07	1.19
Rep. 5	1.00	1.04	1.12	1.22

Table 3.5: Normalized average CV values acquired through direct contact with the skin during the first experiment.

data in order to investigate the two factors. The statistical test resulted "non-significant" for the measurement method (p-value = 0.71) and "significant" for the level of supplied force (p-value = $3.04 \cdot 10^{-14}$).

	25% weight	50% weight	75% weight	100% weight
Rep. 1	1.00	1.04	1.16	1.23
Rep. 2	1.00	1.06	1.12	1.21
Rep. 3	1.00	1.01	1.03	1.24
Rep. 4	1.00	1.04	1.16	1.20
Rep. 5	1.00	1.10	1.15	1.29

Table 3.6: Normalized average CV values acquired through contact-less sensing during the first experiment.

3.2.2   Second experiment

During the second experiment, acquisitions were organized in a separated recording for each force level and for each subject. Recordings from subject 1 had to be discarded. The quality of the signal was affected by strong motion artifacts. An error in the positioning of the electrodes is the most-likely cause of this data loss. Data from the remaining eight subjects were fed into the algorithm described in *3.1.2*, and the result was a CV value for each subject and for each force level. One average CV value out of the two repetitions was considered for each subject. Results are reported in table 3.7 and represented in a box plot in figure 3.22. As done for the first experiment, CV values were normalized before further analyses, and they are reported in table 3.8 and represented in a box plot in figure 3.23. Then, a one-way ANOVA was performed on the normalized CVs, but in contradiction with results from the first experiment the level of supplied force was not significant (p-value = 0.51). Finally, a two-samples t-test was performed considering the lowest force level and the highest force level. The null hypothesis was rejected; thus, the means of the two considered CV sets resulted significantly different.
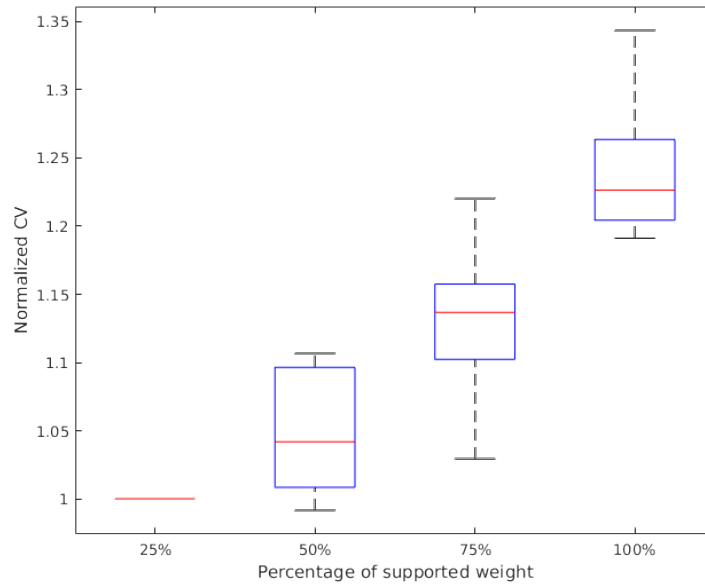
Figure 3.21: Box plot of the complete set of normalized CVs from the first experiment.
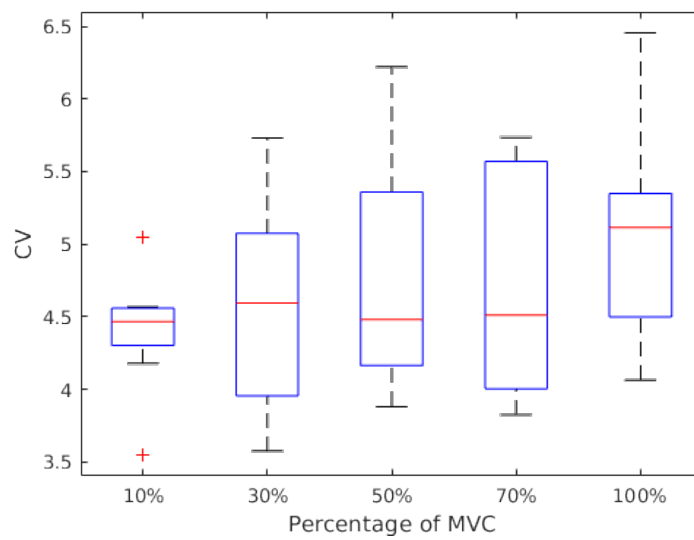
Figure 3.22: Box plot of the complete set of CVs from the second experiment.

	10% MVC	30% MVC	50% MVC	70% MVC	100% MVC
Subject 2	4.55	4.91	4.66	4.24	4.06
Subject 3	3.55	3.57	4.09	4.10	5.08
Subject 4	4.42	3.93	3.88	3.82	4.19
Subject 5	4.43	5.24	6.06	5.61	6.46
Subject 6	5.05	3.98	4.49	5.53	5.37
Subject 7	4.18	5.73	6.22	5.73	4.81
Subject 8	4.57	4.79	4.24	3.90	5.15
Subject 9	4.50	4.40	4.47	4.79	5.33

Table 3.7: Average CV values acquired through contact-less sensing during the second experiment. CV values are expressed in [m/s].

	10% MVC	30% MVC	50% MVC	70% MVC	100% MVC
Subject 2	1.00	1.08	1.02	0.93	0.89
Subject 3	1.00	1.01	1.15	1.16	1.43
Subject 4	1.00	0.89	0.88	0.86	0.95
Subject 5	1.00	1.18	1.37	1.27	1.46
Subject 6	1.00	0.79	0.89	1.10	1.06
Subject 7	1.00	1.37	1.49	1.37	1.15
Subject 8	1.00	1.05	0.93	0.85	1.13
Subject 9	1.00	0.98	0.99	1.06	1.18

Table 3.8: Normalized average CV values acquired through contact-less sensing during the second experiment.

3.3   Discussion

The usefulness of average muscle fibers' CV estimation and its applications have been extensively discussed in *1* and in *3*. However, state-of-the-art systems able to compute this feature are not practical nor easy-to-use, and they require a strong expertise for the correct positioning of the electrodes.
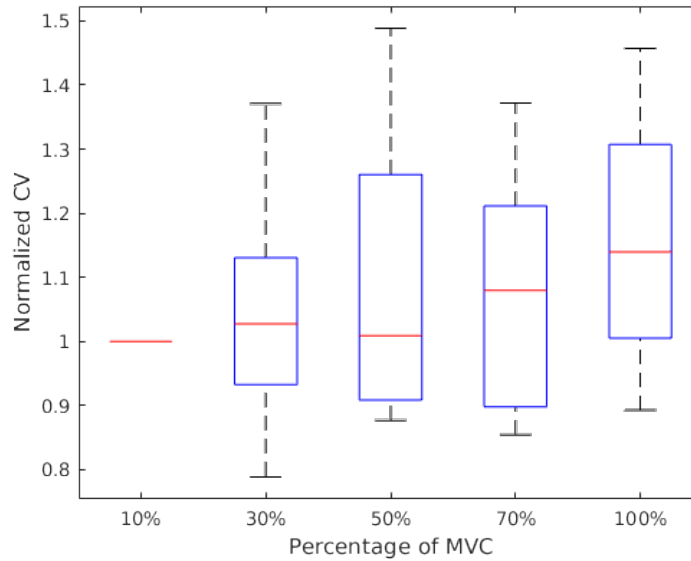
Figure 3.23: Box plot of the complete set of normalized CVs from the second experiment.

The aim of the study was to develop an acquisition system capable of estimating muscle fibers' CV, but exempt from the practical limitations that affects common sEMG acquisition [12].

An acquisition system composed of electrodes, hardware and software has been developed. It is capable of estimating average muscle fibers' CV and of appreciating its variation with different force level supplied by the sensed muscle. Also, it does not require any kind of manual calibration, nor any skin preparation, nor any conductive gel to be placed on the skin. Moreover, the system is able to estimate muscle fibers' average CV on top of a thin layer of clothing, without a direct contact with subject's skin. However, the estimated value of muscle fibers' average CV is strongly dependent on electrodes array orientation with respect to muscle fibers orientation. The estimated CV will result in a higher value if the two elements are not aligned. Each experiment was performed with the aim of obtaining the best alignment. Information supplied by [70] were followed for the positioning, but a gold standard was not available. Thus, it was not possible to concretely

verify that the value estimated by the developed system coincided with the actual average CV value. Nevertheless, having an easy-to-use and practical system able to estimate average CV enables the investigation of the relationship between the extent of the effort sustained by the muscle and the variation in the average CV, as stated in *3*. In fact, a simple normalization that was performed for each recording avoids the described uncertainty due to the alignment. As described in *3.2*, each CV value was divided by the CV corresponding to the the lowest force supplied by the muscle during the respective recording. Moreover, this normalization enables the results comparison between different subjects with different fibers and array alignments, as Pozzo et al. performed in [62].

The performance of the system were investigated through two experiments. In the first place, the reproducibility of the measurement on one subject during several repetitions was investigated. The experiment regarded acquisitions with direct contact on the skin and contact-less acquisitions. The employed system was the one described in *3* in both cases, the only difference was a sheet of 100% cotton fabric in between the electrodes and the skin in the contact-less acquisitions. Results were statistically studied through a two-way unbalanced ANOVA. As expected from the theory [11], the force level resulted significant for the estimated average CV value. Furthermore, the measurement method (contact or contact-less) resulted non-significant for the CV. Statistical results are in accordance with results from [62]. A further comparison with the work of Pozzo and co-workers is shown in figure 3.24. Results of measured CV from right vastus medialis are adapted from [62] and plotted with results obtained in the first experiment from the investigated subject. Average CV values over the repetition sets are computed from results in *3.2.1* and plotted. The graph shows that the results from the two works are numerically compatible. In conclusion, the acquisition system performed in line with expectations during the first experiment.

As far as the second experiment is concerned, the reproducibility of the measurement over a pool of subjects was investigated. The system described
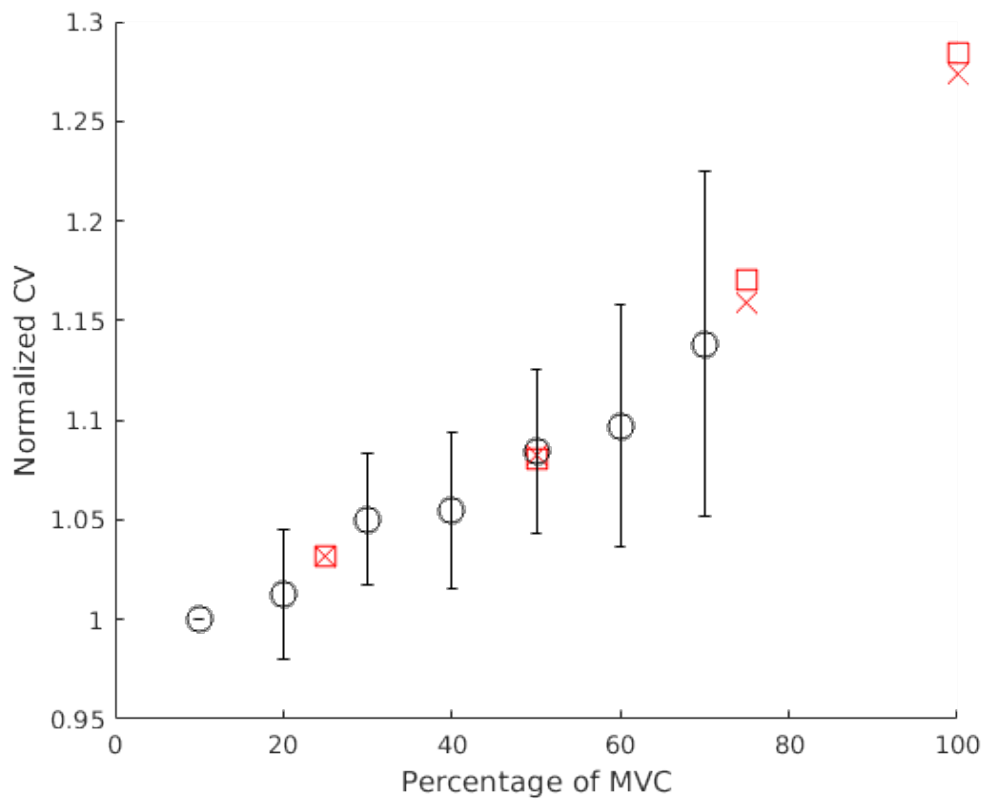
Figure 3.24: Comparison between results from [62] and results from *3.2.1*. In black the former with the respective standard deviation. Red square markers correspond to direct-contact data, red cross markers correspond to contactless data.

in *3* acquired contact-less data from nine healthy people. Results were statistically studied through a one-way ANOVA. The outcome was in contradiction with results from the previous experiment, because force level resulted non-significant for the estimated average CV. Further, a two-sample t-test was performed and data corresponding to the lowest force level and the highest force level were compared. The outcome was in line with the theory, the null hypothesis was rejected and the force level resulted significant.

Several factors could have influenced the result of the second experiment. In particular, the design of the experimental setup plays an important role in the acquisition of meaningful data. During the second experiment, subjects had more degree of freedom in the motion of the leg. The pulling of the belt, as described in *3.1.3*, was not restricted, thus small lateral movements were possible. Consequently, subjects' nervous system could have applied different strategies in order to provide the requested force. Depending on subject-related factors, a considerable part of the requested force could have been supplied from muscles other than vastus medialis. Conversely, the first experimental setup, described in *3.1.3*, had less degree of freedom because no legs movements were necessary to acquire data. For the sake of clarity, a comparison between results acquired in the second experiment and results acquired in [62] is shown in figure 3.25.

The novelty of the designed system lies in combining capabilities of state-of-the-art array-based EMG acquisition systems with capacitive-sensing technology. The results reported in the dissertation are encouraging. Nevertheless, further investigations and tests need to be performed to validate the effectiveness and the robustness of the system.
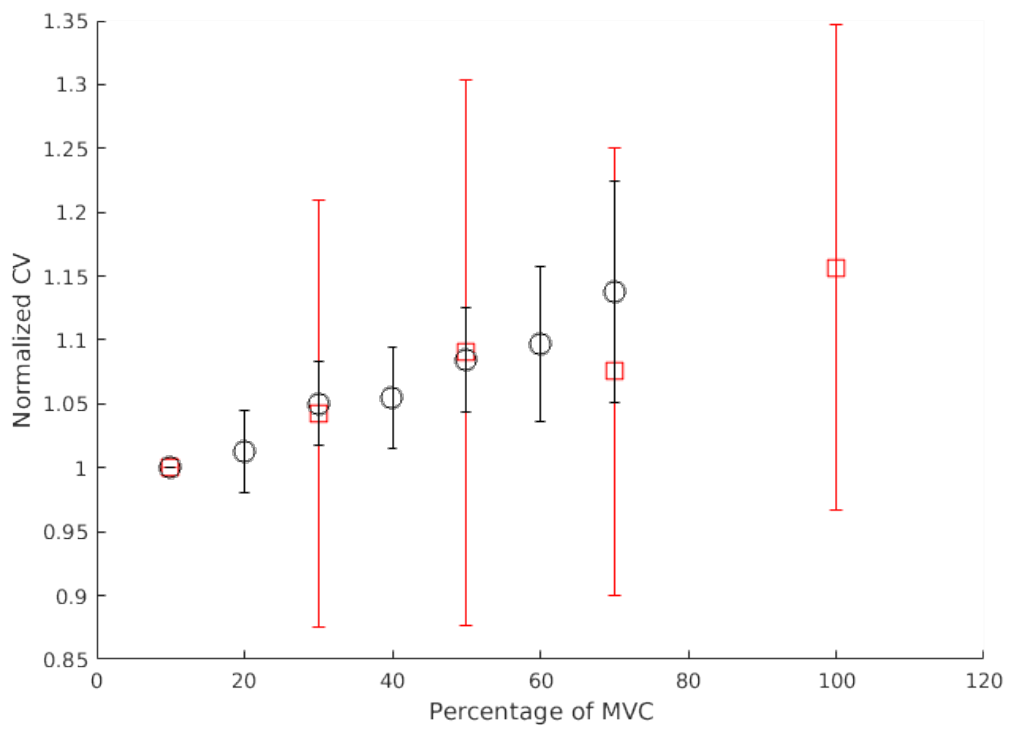
Figure 3.25: Comparison between results from [62] and results from *3.2.2.* In black the former with the respective standard deviation. In red the latter with the respective standard deviation.

Chapter 4

Conclusion

The purpose of the dissertation is investigating new tools for wearable-device-control systems based on electromyographic (EMG) signals. In particular, the detection of muscle activity and the estimation of force intention are investigated. In both cases, tools must be reliable and robust even in non-clinical environments. They must not require any skin preparation nor manual calibration, and they must not need any specific knowledge for exact electrodes positioning. Moreover, they must be able to operate with EMG signals acquired over clothes. Finally, tools must be suitable to long-term measurements and keep their reliability over time. The described requirements clearly distinguish the present work from state-of-the-art products.

Chapter *2* reports the development of the first tool: an offline algorithm able to reliably detect EMG activation through contact-less measurements. The algorithm was tested on experimental data with the help of a gold standard, and results are comparable to algorithms existing in literature for direct-contact measurements. In particular, the proposed method demonstrates robustness against the highly variable range of considered SNRs due to the capacitive nature of the employed acquisition system.

Chapter *3* reports the development of the second tool: a capacitive-sensing array-based EMG acquisition system composed of sensors, hardware and software. To the best of author's knowledge, no other system of such a

nature have been proposed in literature until now. The aim of this second tool is to collect information about the force intention of the user through the estimation of average muscle fibers' conduction velocity. The designed system performed in line with expectations in the first experiment. It was able to assess average conduction velocity and to appreciate its variation with the force supplied by the sensed muscle. When a pool of different subjects was involved, the system was affected by uncontrolled influencing factors. Thus, results were not statistical significant. Nevertheless, performance are strongly encouraging and further tests need to be done to proof the effectiveness and robustness of the designed system.

Developed tools were designed according to requirements previously stated. Their performance were evaluated and compared with some state-of-the-art tools existing in literature. A considerable subject-related variability has been highlighted in both cases. This influence has a critical importance, and need to be addressed in future designs and studies. Studies performed in the present dissertation open up the way for further development of the proposed tools. A first natural evolution of both the EMG-activity-detection algorithm and the capacitive-sensing array-based EMG acquisition system would be real-time operation and results. As far as the second tool is concerned, it would be possible to increase the effectiveness and the robustness of the system by means of an electrodes two-dimensions matrix instead of a single-dimension array. State-of-the-art direct-contact solutions already employ matrix of electrodes to investigate surface-EMG. Contact-less technology would benefit from this development in term of accuracy and reliability. Furthermore, the higher design complexity would be compensated by the possibility of exploiting flexible-PCB manufacturing technology to realize the electrodes. Thanks to that technology, a higher integration level in terms of hardware would be easy to achieve with a considerable improvement in the signal-to-noise ratio of the whole acquisition system.

In conclusion, the development of strongly robust and reliable tools able to detect EMG activity and to assess user's force intention will bring about

strong improvements in human-machine interfaces. Current EMG-based solutions are unpractical and they can not be operated by unexperienced users. Easy-to-use and user-friendly devices will grant the investigated technology the access to many consumer and diagnostic applications, such as wearable assistive and rehabilitation robotics or long-term diagnostic studies.

Appendix A

Printed Circuit Board layout

The circuit described in *3.1.1.2* has been designed and built. The necessary components are listed in table A.1.

Name	Description	Value	Package
R1	Resistor 1%	1GΩ	2512
R4	Resistor 5%	100Ω	0805
R5	Resistor 5%	10KΩ	0805
R6	Resistor 5%	330KΩ	0805
R7	Resistor 5%	100Ω	0805
R8	Resistor 1%	1GΩ	2512
R11	Resistor 5%	100Ω	0805
R12	Resistor 5%	10KΩ	0805
R13	Resistor 5%	330KΩ	0805
R14	Resistor 5%	100Ω	0805
R15	Resistor 5%	1KΩ	0805
R16	Resistor 5%	33KΩ	0805
R17	Resistor 5%	0Ω	0805
R18	Resistor 5%	330KΩ	0805
R19	Resistor 5%	33KΩ	0805
C1	Capacitor 10%	100nF	0805

C2	Capacitor 10%	100nF	0805
C3	Capacitor 10%	10nF	0805
C5	Capacitor 10%	100nF	0805
C6	Capacitor 10%	100nF	0805
C7	Capacitor 10%	1nF	0805
C8	Capacitor 10%	100nF	0805
C9	Capacitor 10%	100nF	0805
C10	Capacitor 10%	10nF	0805
C12	Capacitor 10%	100nF	0805
C13	Capacitor 10%	100nF	0805
C14	Capacitor 10%	1nF	0805
C15	Capacitor 10%	100nF	0805
C16	Capacitor 10%	100nF	0805
C17	Capacitor 10%	100nF	0805
C18	Capacitor 10%	100nF	0805
C19	Capacitor 10%	100nF	0805
C20	Capacitor 10%	1nF	0805
U1	LMP7721MA/NOPB		SOIC-8
U2	LMP7715MF/NOPB		SOT-23-5
U3	LMP7721MA/NOPB		SOIC-8
U4	LMP7715MF/NOPB		SOT-23-5
U5	INA118U		SOIC-8
U6	OPA2350UA		SOIC-8
U7	1N4148WS		SOD-323F-2
U8	1N4148WS		SOD-323F-2
U9	Dual Switch		DIP-6
J1	PCB Battery Holder		Surface Mount
J2	PCB Battery Holder		Surface Mount
J3	MCX Connector jack		Surface Mount
J4	MCX Connector jack		Surface Mount

J5	MCX Connector jack		Surface Mount

Table A.1: Components' list.

Figure A.1, figure A.2 and figure A.3 show the top layers of the designed PCB. Figure A.4 shows the bottom layers of the designed PCB. As suggested in [64], no solder mask was placed on the input signal traces. This prevents static charge from accumulating. Following the same document, a guarding ring was designed around each impedance adapters and no ground plane was placed.

Figure A.1: Top copper.

Figure A.2: Top copper with silkscreen.
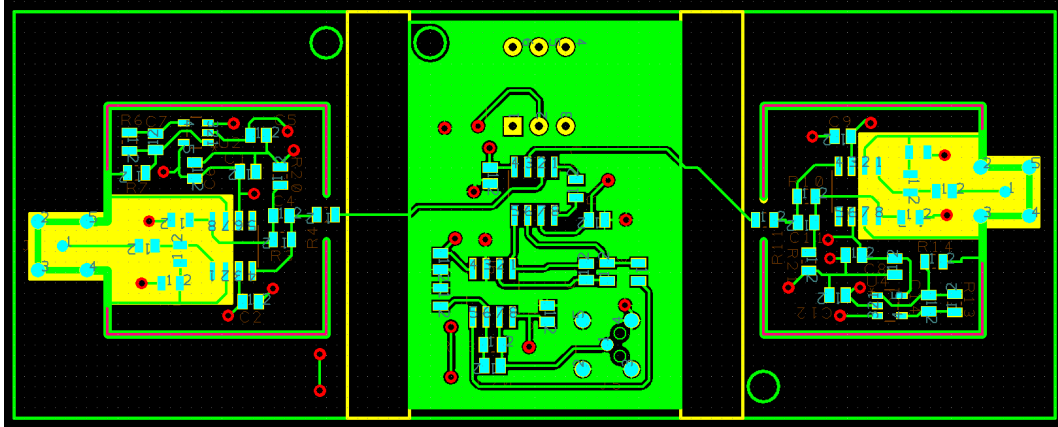
Figure A.3: Top copper with silkscreen and solder-free areas (in yellow).
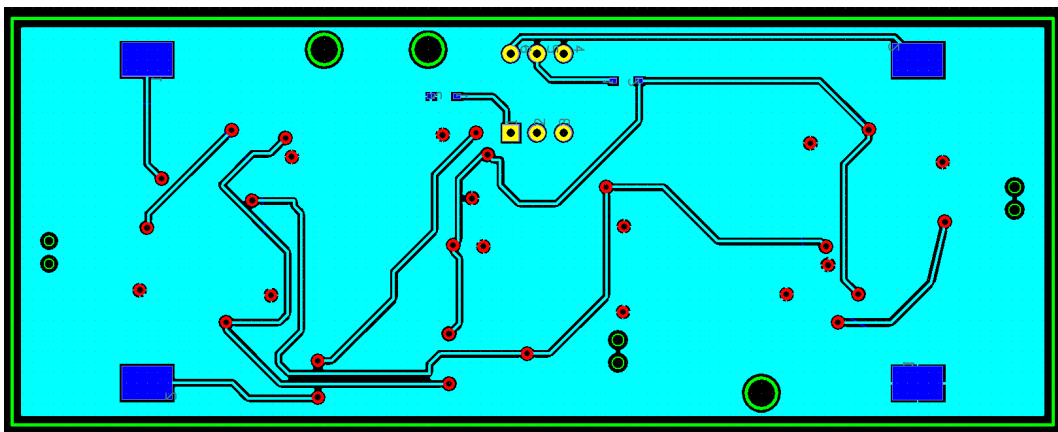
Figure A.4: Bottom copper with silkscreen and solder-free areas.

Appendix B

Force visual feedback

In order to perform the experiment described in *3.1.3*, each subject needed a visual feedback of the force that he or she was applying by pulling the belt with his or her leg. A simple and inexpensive system was designed to give a real-time and reliable output. A schematic view of the system is shown in figure B.1.

The belt that the subject was asked to pull was connected to a load cell. The load cell was firmly fixed to the experimental frame, thus there was no relative motion between the subject and the load cell. This device is composed of a metal rigid frame and two strain gauges with opposite behavior. One increase its resistance when the metal frame is bended and the second decreases its resistance when a bending occur. The two elements were configured as two arms of a wheatstone bridge, which enable the detection of small variations in their resistance. Moreover, the wheatstone bridge includes a variable resistor in order to calibrate the output base line. The realized circuit is shown in figure B.2.

The signal from the wheatstone bridge is picked up from an instrumentation amplifier (AD623). In order to provide the subject with an understandable feedback, the gain of the AD623 was configured through a variable resistor directly during the experiment. Finally, the output of the instrumentation amplifier was visualized through a portable oscilloscope and shown to
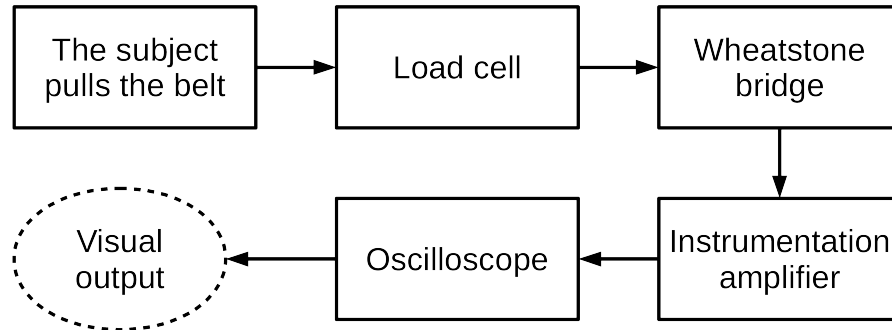
Figure B.1: Force visual feedback system's block diagram.
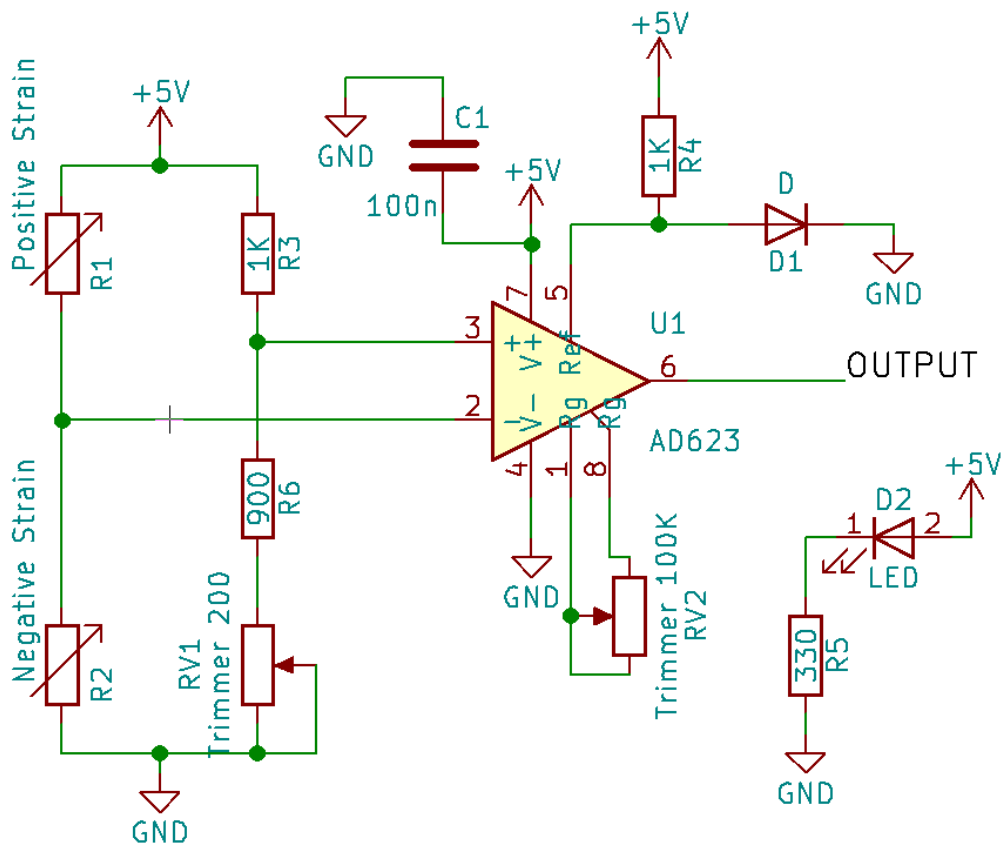
Figure B.2: Force visual feedback system's circuit.

the subject. A picture of the realized system is shown in figure B.3. Eventually, a pulley was inserted in the connection between the subject and the load cell. Its purpose was to proportionally reduce the amount of force measured by the device and to stay inside load cell's safe usage limit (500 N). In this case, the load cell measured half of the force applied by the subject.

A list of the necessary components is provided in table B.1.

Name	Description	Value	Package
R1	Positive-coeff. strain gauge	1KΩ	Inside load cell
R2	Negative-coeff. strain gauge	1KΩ	Inside load cell
R3	Resistor 1%	1KΩ	Through-hole
R4	Resistor 1%	1KΩ	Through-hole
R5	Resistor 1%	330Ω	Through-hole
R6	Resistor 1%	900Ω	Through-hole
RV1	Variable resistor	200Ω	Through-hole
RV2	Variable resistor	100KΩ	Through-hole
C1	Capacitor 10%	100nF	0805
U1	AD623		SOIC-8
D1	1N4148		Through-hole
D2	Red led diode		Through-hole

Table B.1: Force visual feedback components' list.
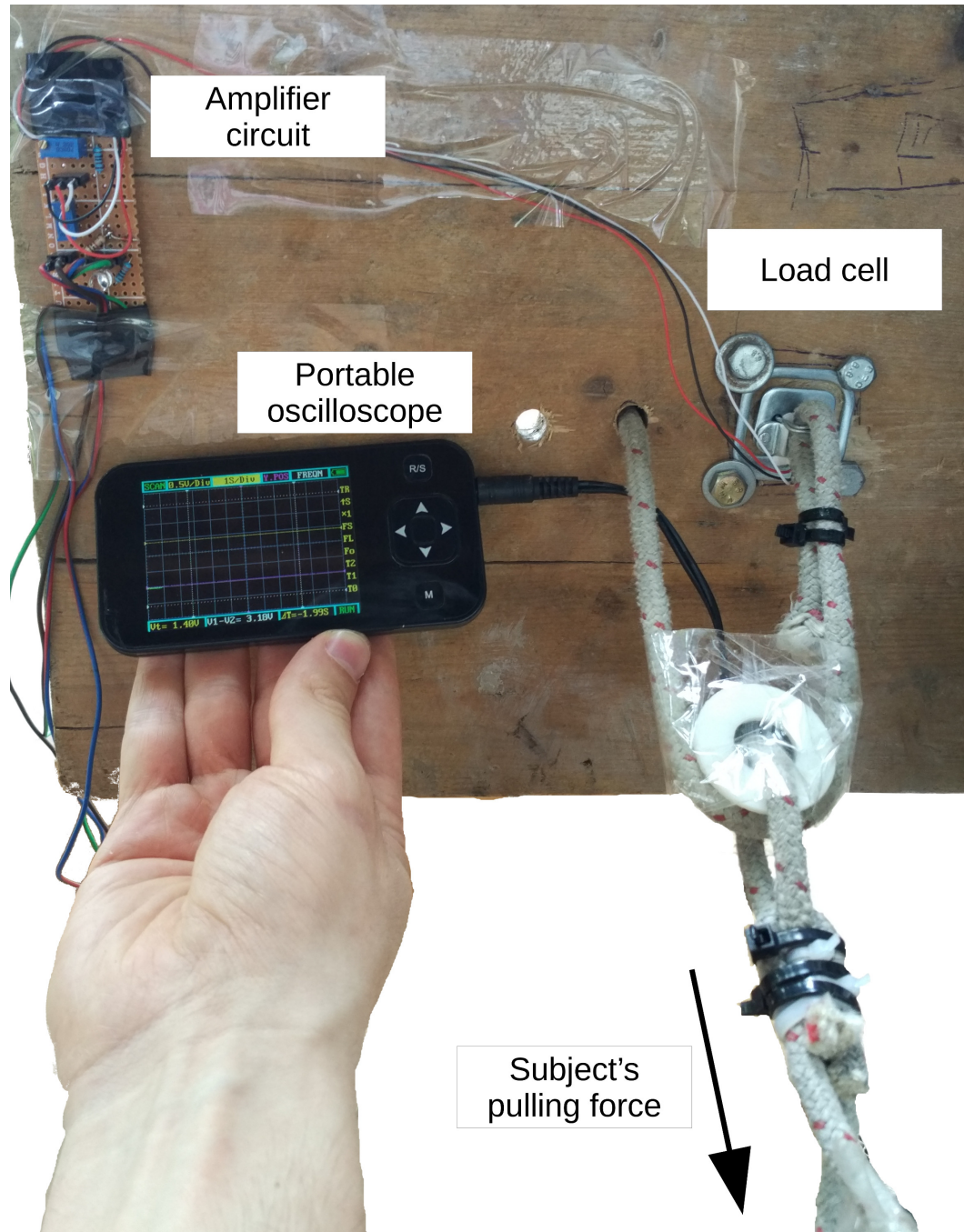
Figure B.3: Force visual feedback system's picture.

Bibliography

[1] Shumway-Cook, A.; Woollacott, M. H. Physiology of motor control. In Motor Control. 4th ed., Williams & Wilkins: Philadelphia/Baltimore USA 2012, pp. 45-83.

[2] Benedetti, M. G. Muscle activation intervals and EMG envelope in clinical gait analysis. IEEE Engineering in Medicine and Biology 2001, 20 (6), pp. 33-34.

[3] Perry, J. The contribution of dynamic electromyography to gait analysis. Gait Analysis in the Science of Rehabilitation. Washington 1998. p. 33-48.

[4] Benedetti, M.G.; Bonato, P.; Catani, F.; D'Alessio, T.; Knaflitz, M.; Marcacci, M. Myoelectric activation pattern during gait in total knee replacement: relationship with kinematics, kinetics and clinical outcome. IEEE Transaction of Rehabilitation Engineering 1999, 7 (2), pp. 140-149.

[5] Prilutsky, B.I.; Gregor, R.J.; Ryan, M.M. Coordination of two-joint rectus femoris and hamstrings during the swing phase of human walking and running. Experimental Brain Research 1998, 120, pp. 479-486.

[6] Wu, Y.; Martinez, M. A. M.; Orizaola, P. Overview of the Application of EMG Recording in the Diagnosis and Approach of Neurological Disorders in New Frontiers of Clinical Research, InTech 2013. DOI: 10.5772/56030. Available from:

http://www.intechopen.com/books/electrodiagnosis-in-new-frontiers-of-clinical-research/overview-of-the-application-of-emg-recording-in-the-diagnosis-and-approach-of-neurological-disorders.

[7] Gorpura, R. A. R. C.; Bandara, D. S. V.; Gunasekara, J. M. P.; Javawardane, T. S. S. R. Electrodiagnostics in New Frontiers of Clinical Research, InTech 2013. DOI: 10.5772/56174. Available from: http://www.intechopen.com/books/electrodiagnosis-in-new-frontiers-of-clinical-research/recent-trends-in-emg-based-control-methods-for-assistive-robots

[8] Wall, A.; Borg, J.; Palmcrantz, S. Clinical application of the Hybrid Assistive Limb (HAL) for gait training-a systematic review. Frontiers in Systems Neuroscience 2015, 9, article 48.

[9] Li, G.; Kuliken, T. A. EMG pattern recognition control of multifunctional prostheses by transradial amputees. In Proceeding IEEE Engineering in Medicine and Biology Society, Minesota, USA, 2009.

[10] Broman, H.; De Luca, C. J.; Mambrito, B. Motor unit recruitment and firing rates interaction in the control of human muscles. Brain Resarch 1985, 337: 311-319.

[11] Henneman, E.; Somjen, G.; Carpenter, D. O. Functional significance of cell size in spinal motoneurons. Department of Physiology, Harvard Medical School, Boston 1964.

[12] Ueno, A.; Akabane, Y.; Kato, T.; Hoshino, H.; Kataoka, S.; Ishiyama, Y. Capacitive sensing of elecrocardiographic potential through cloth from the dorsal surface of the body in a supine position: A preliminary study, IEEE Transaction on Biomedical Engineering 2007, 54(4). pp. 759-766.

[13] Ueno, A.; Uchikawa, Y.; Noshiro, T. A capacitive sensor system for measuring Laplacian electromyogram through cloth: a pilot study. IEEE Engineering in Medicine and Biology Society, 2007, pp. 5732-5.

[14] Ohtsu, M.; Fukuoka, Y.; Ueno, A. Underwater electromyographic measurement using a waterproof insulated electrode, Advanced Biomed Engineering 2012, 1, pp. 81-88.

[15] Luna-Lozano, P.S.; Pallas-Areny, R. Microphonics in bio-potential measurements with capacitive electrodes. In Proceedings of IEEE on Engineering in Medicine and Biology Society 2010, pp 3487-90.

[16] Linz, T.; Gourmelon, L.; Langereis, G. Contactless EMG sensors embroided onto textile. In: Leonhardt S., Falck T., Mahonen P. (eds) 4th International Workshop on Wearable and Implantable Body Sensor Networks (BSN 2007). IFMBE Proceedings, vol 13. Springer, Berlin, Heidelberg

[17] Gourmelon, L.; Langereis, G. Contactless sensors for surface electromyography. In: In Proceedings of IEEE on Engineering in Medicine and Biology Society 2006, pp 2514-7.

[18] Merletti, R.; Farina, D.; Gazzoni, M. Surface EMG: The issue of electrode location. Journal of Electromyography and Kinesiology 2009, 13:37-47.

[19] Rojas-Martinez, M.; Mananas, M. A.; Alonso, J.F. High-density surface EMG maps from upper-arm and forearm muscles. Journal of neuroengineering and Rehabilitation 2012, 9:85.

[20] Micera, S.; Vannozzi, G.; Sabatini, A. M.; Dario, P. Improving detection of muscle activation intervals. IEEE Engineering in Medicine and Biology 2001, 20 (6), pp. 38-46.

[21] Bogey R.A.; Barnes, L.A.;Perry, J. Computer algorithms to characterize individual subject EMG profiles during gait. Archives of Physical Medicine and Rehabilitation 1992, 73, pp. 835-841.

[22] Hodges, P.W.; Bui, B.H. A comparison of computer-based methods for determination of onset of muscle contraction using electromyography.

Electroencephalography and Clinical Neurophysiology 1996, 101, pp. 511-519.

[23] Xu, L.; Adler, A. An improved method for muscle activation detection during gait. In Proceedings of IEEE Canadian Conference on Electrical and Computer Engineering, Canada 2004, pp. 357-360.

[24] Bonato, P.; D'Alessio, T.; Knaflitz, M. A statistical method for the measurement of muscle activation intervals from surface myoelectric signal during gait. IEEE Transaction on Biomedical Engineering 1998, 45 (3), pp. 287-299.

[25] Micera, S.; Sabatini, A.M.; Dario, P. An algorithm for detecting the onset of muscle contraction by EMG signal processing. In Medical Engineering and Physics 1997, 16, pp. 70-76.

[26] Merlo, A.; Farina, D.; Merletti, R. A fast and reliable technique for muscle activity detection from surface EMG signals. IEEE Transaction on Biomedical Engineering 2003, 50 (3), pp. 316-323.

[27] Neto, O.P.; Marzullo, A.C.D. Wavelet transform analysis of electromyography Kung Fu strikes data. Journal of Sports Science and Medicine 2009, 8 (3), pp. 25-28.

[28] Kumar, S.; Prasad, N. Torso muscle EMG profile differences between patients of back pain and control. Clinical Biomechanics 2010, 25 (2), pp. 103-109.

[29] Kumar, D.K.; Pah, N.D.; Bradley, A. Wavelet analysis of surface electromyography to determine muscle fatigue. IEEE Transaction on Neural Systems and Rehabilitation Engineering 2003, 11 (4), pp. 400-406.

[30] Hussain, M.S.; Reaz, M.B.I.; Mohd-Yasin, F.; Ibrahimy, M.I. Electromyography signal analysis using wavelet transform and higher order statistics to determine muscle contraction. Expert Systems with Application 2009, 26 (1), pp. 35-48.

[31] Wang, G.; Wang, Z.; Chen, W.; Zhuang, J. Classification of surface EMG signals using optimal wavelet packet method based on Davies-Bouldin criterion. Medical and Biological Engineering and Computing 2006, 44 (4), pp. 865-872.

[32] Englehart, K.; Hudgins, B.; Parker, P.A. A wavelet-based continuous classification scheme for multifunction myoelectric control. IEEE Transaction on Biomedical Engineering 2001, 48 (3), pp. 302-311.

[33] Chu, J.U.; Moon, I.; Mun, M.S. A real-time EMG pattern recognition system based on linear-nonlinear feature projection for a multifunction myoelectric control. IEEE Transaction on Biomedical Engineering 2006, 53 (11), pp. 2232-2239.

[34] Chu, J.U.; Moon, I.; Lee, Y.J.; Kim, S.K.; Mun, M.S. A supervised feature-projection-based real-time EMG pattern recognition for multifunction myoelectric hand control. IEEE/ASME Transaction on Mechatronics 2007, 12 (3), pp. 282-290.

[35] Boostani, R.; Moradi, M.H. Evaluation of the forearm EMG signal features for the control of a prosthetic hand. Physiological Measurement 2003, 24 (2), pp. 309-319.

[36] Phinyomark, A.; Limsakul, C.; Phukpattaranont, P. Application of wavelet analysis in EMG feature extraction for pattern classification. Measurement Science Review 2011, 11(2), pp. 45-52.

[37] De Luca, C. J. The Use of Surface Electromyography in Biomechanics. Journal of Applied Biomechanics 1997, 13, pp. 135-163.

[38] Sparto, P. J.; Parnianpour, M.; Barria, E. A.; Jagadeesh, J.M. Wavelet Analysis of Electromyography for Back Muscle Fatigue Detection during Isokinetic Constant-Torque Exertions. Spine 1999, 24, pp. 1791-1798.

[39] Bonato, P.; Roy, S.H.; Knaflitz, M.; De Luca, C.J. Time-Frequency Parameters of the Surface Myoelectrictigue during Cyclic Dynamic Contractions , IEEE Transactions on Biomedical Engineering 2001, 48, pp. 745-753.

[40] Bigliassi, M.; Scalassara, P. R.; Kanthack, T. F. D.; Abrao, T.; de Moraes, A. C.; Altimari, L. R. Fourier and Wavelet spectral analysis of AMG signal in 1-km cycling time trial, Applied Mathematics 2014, 5, pp. 1878-1886.

[41] Maquet. Available online: https://www.aic.cuhk.edu.hk

[42] Ueno, A.; Yamaguchi, T.; Iida, T.; Fukuoka, Y.; Uchikawa, Y.; Noshiro, M. Feasibility of Capacitive Sensing of Surface Electromyographic Potential through Cloth, Sensors and Materials 2012, 24(6), pp. 335-346.

[43] Seniam. Available online: http://www.seniam.org/.

[44] Wiener, N. Extrapolation, interpolation, and smoothing of stationary time series. The MIT Press, Cambridge, MA, USA, 1964.

[45] Scalart, P. Speech enhancement based on a priori signal to noise estimation. In Proceedings of IEEE International Conference on Acoustics, Speech, and Signal Processing, Atlanta, GA, USA, 1996, pp.629-632.

[46] Aschero, G.; Gizdulich, P. Denoising of surface EMG with a modified Wiener filtering approach. Journal of Electromyography and Kinesiology 2010, 20 (2), pp. 366-373.

[47] Varanini, M. Time-Frequency Representation. In Advanced Methods of Biomedical Signal Processing. 1st ed., John Wiley & Sons Inc, New Jersey, USA, 2009, pp. 203-207.

[48] Chang, C. Progressive coding for spectral signatures. In Hyperspectral data processing. 1st ed., John Wiley & Sons Inc, New Jersey, USA, 2009, pp. 741-760.

[49] Azegami, M.; Yanagihashi, R.; Miyoshi, K.; Akahane, K.; Ohira, M.; Sadoyama, T. Effects of multi-joint angle changes on EMG activity and force of lower extremity muscles during maximum isometric leg press exercises. Journal of Physical Therapy Science 2007, 19(1), pp. 65-72.

[50] Winter D. A. Muscle mechanics. In Biomechanics and motor control of human movement. 4th ed., John Wiley & Sons Inc: New Jersey, USA, 2009, pp. 224-240.

[51] Moore, K. L.; Dalley, A. F.; Agur, A. M. R. Lower Limb. In Moore Clinically oriented anatomy. 7th ed., Williams & Wilkins: Philadelphia/Baltimore USA, 2014, pp. 545-562.

[52] Zhu, W.; Zeng, N.; Wang, N. Sensitivity, specificity, accuracy, associated confidence interval and ROC analysis with practical SASÂ® implementation. In Proceedings of NESUG: health care and life science, 2010, pp. 1-9.

[53] Xu, Q.; Quan, Y.; Yang, L.; He, J. An adaptive algorithm for the determination of the onset and offset of muscle contraction by EMG signal processing. IEEE Transactions on Neural Systems and Rehabilitation Engineering 2013, 21 (1), pp. 65-73.

[54] Li, X.; Aruin, A. Muscle activity onset time detection using teager-kaiser energy operator. In Proceedings of Engineering in Medicine and Biology Society, 2005 (7), pp. 7549-52.

[55] Pasinetti, S.; Lancini, M.; Bodini, I.; Docchio, F. A Novel Algorithm for EMG Signal Processing and Muscle Timing Measurement. IEEE Transactions on Instrumentation and Measurement 2015, 64 (11), pp. 2995-3004.

[56] Micera, S.; Sabatini, AM.; Dario, P. An algorithm for detecting the onset of muscle contraction by EMG signal processing. Medical Engineering & Physics 1998, 20(3), pp. 211-215.

[57] De Luca, C.J.; Gilmore, L.D.; Kuznetsov, M.; Roy, S.H. Filtering the surface EMG signal: Movement artifact and baseline noise contamination. Journal of Biomechanics 2010, 43, pp. 1573-1579.

[58] Day, S. Important Factors in Surface EMG Measurement. Bortec Biomedical LTD 2002.

[59] Angkoon, P.; Sirinee, T.; Huosheng, H.; Pornchai, P.; Chusak, L. (2012). The Usefulness of Mean and Median Frequencies in Electromyography Analysis, Computational Intelligence in Electromyography Analysis - A Perspective on Current Applications and Future Challenges, Dr. Ganesh R. Naik (Ed.), InTech, DOI: 10.5772/50639. Available from: https://www.intechopen.com/books/computational-intelligence-in-electromyography-analysis-a-perspective-on-current-applications-and-future-challenges/the-usefulness-of-mean-and-median-frequencies-in-electromyography-analysis

[60] Farina, D.; Pozzo, M.; Merlo, E.; Bottin, A. and Merletti, R. (2004). Assessment of average muscle fiber conduction velocity from surface EMG signals during fatiguing dynamic contractions. IEEE Trans Biomed Eng., 51(8): 1383-93.

[61] Farina, D.; Muhammad, W.; Fortunato, E.; Meste, O.; Merletti, R. and Rix, H. (2001). Estimation of single motor unit conduction velocity from surface electromyogram signals detected with linear electrode arrays. Med Biol Eng Comput., 39(2): 225-36.

[62] Pozzo, M.; Merlo, E.; Farina, D.; Antonutto, G.; Merletti, R. and Prampero, P. E. D. (2004). Muscle-fiber conduction velocity estimated from surface emg signals during explosive dynamic contractions. Muscle Nerve, 29: 823-833.

[63] Huppertz, H.-J.; Disselhorst-klug, C.; Silny, J.; Rau, G. and Heimann G. (1997). Diagnostic yield of noninvasive high spatial resolution electromyography in neuromuscular diseases. Muscle Nerve, 20: 1360-1370.

[64] Grohe, P. (2010). LMP7721 Multi-Function Evaluation Board Users' Guide. National Semiconductor, rev. 1.

[65] Texas Instruments (2014). LMP7721 3-Femtoampere Input Bias Current Precision Amplifier. Available online: http://www.ti.com/lit/ds/symlink/lmp7721.pdf 10/12/2016.

[66] Stitt, M. (1991). Ac coupling instrumentation and difference amplifiers. Burr-Brown. Available online: http://www.ti.com/lit/an/sboa003/sboa003.pdf 10/12/2016.

[67] Farina, D.; Merletti, R. (2004). Methods for estimating muscle fibre conduction velocity from surface electromyographic signals. Med. Biol. Eng. Comput., 42(4):432-45.

[68] Mesin, L.; Merletti, R.; Rainoldi, A. (2009). Surface EMG: The issue of electrode location. Journal of Electromyography and Kinesiology, 19:719-26.

[69] Farina, D.; Merletti, R. (2000). Comparison of algorithms for estimation of EMG variables during voluntary isometric contractions. Journal of Electromyography and Kinesiology, 10:337-49.

[70] Rainoldi, A.; Melchiorri, G.; Caruso, I. (2003). A method for positioning electrodes during surface EMG recordings in lower limb muscles. Journal of Neuroscience Methods, 134:37-43.